Content of this file:

- Response to the editor
- Response to Referee #2
- Response to Referee #3
- Track changes of manuscript

Below, the black is the comment and the blue is our response.

Response to the editor

Thank you for uploading the revision and replies to the referee comments. I think the manuscript has much improved, but at this stage there are still some issues that prevent your work to be published in The Cryosphere. I have copied the referee comments below for your convenience.

Referee #2 suggest to look into ERA5 for the precipitation analysis. I support this, but it is not a necessary requirement for publication, as long as you can provide convincing arguments why results are not expected from ERA5 are not expected to be significantly different.

We have updated the relevant part (Fig. 2, Fig. S5, Section 2.4) with the EAR5 precipitation product. However, we do not update the validation of the first mode of GRACE. Please refer to our response to the referee for details.

Referee #3 has more substantial and major comments. He/She is correct in saying that EOF modes are always orthogonal and therefore the orthogonality test has little added value. This and the other major comments of R3 need to be addressed.

We still hold a different opinion from referee #3 on the importance of the forward modeling part. I feel the referee thought we directly used the result from the EOF decomposition to do the forward modeling, which is obviously meaningless. In fact, we tested glacier-snow signals with peaks in various months to validate the inversion result, and the orthogonality deteriorated in many cases, so the expectation of "always orthogonal" is invalid. In our view, the forward modeling is as important as the inversion, because it evaluates the uniqueness and credibility of the result. For more details, please refer to the response to referee #3.

Furthermore, I have attached a pdf with my own comments.

Thanks for your work. We understand that it is time consuming for the editor to review a manuscript in person. Your help on the content and the language is highly appreciated. Changes have been made based on your comments, but we have a different idea on the estimation of leakage (see below).

One major shortcoming is that leakage of hydrological signals outside the region of interest seems not to be accounted for. I realize that this will require effort, but at least a quantification of the effect and related uncertainties on the annual mass change should be included.

> *(*comment from your annotation*) This is not what is generally understood by 'leakage'. Leakage usually refers to the effect of hydrological signals outside your region of interest due to the low resolution of GRACE. Since you are only simulating glacier mass changes in the SETP, other signals (such as snowfall/melt) will be partially absorbed as well.*
It's good that you investigate the separation of the modes, but you should also look into the impact of this standard leakage error.

I would like to point out that this is related to the particularity of this study. The "standard leakage error" indicated in your comment is shown in Figure R1(a), where the signal of interest is usually the predominant signal in the region, so the leakage from the interfering signal can be estimated by calculating its proportion in the study region without investigating the details of the interfering signal. This step is carried out in the spatial domain. However, the water storage signal in our study region and surroundings is so significant that it overwhelms other signals in the region (subplot-b), so we must estimate both of them and then separate them. As we wrote in Section 4.1:

Although the first mode is much stronger than the second mode (because the second one is more localized), their signal strength in the glacierized region is comparable on both seasonal and secular temporal scales.

The traditional signal separation in the spatial domain is no longer applicable, since even a slight fraction of leakage would bring in a great uncertainty. However, we found it's feasible to separate the signal in the temporal domain, which is the motivation of this study.

Here, we did not try to separate glacier and snow signals, so the only interfering signal is the hydrological signal. The leakage problem is simplified to the degree of separation of the hydrological signal and the glacier

and snow (GS) signal. Specifically, how much of the hydrological signal leaks into the second mode of the EOF result, and how much of the GS signal leaks into the first mode. Thankfully, we found that the leakage imposes a local pattern on the shape of EOF1 (subplot-c), so we can quantify it based on the spatial pattern of EOF1. Note the shape of hydrological and GS signals has been defined by their corresponding EOF function, which also constrains the spatial pattern of the leakage (so the leakage cannot occur in an arbitrary shape).

Traditionally, the leakage is estimated in the spatial domain regardless of its physical source; while here it is estimated in the perspective of the signal source, which carries specific spatial and temporal characteristics. If the correspondence between the study area and the target signal source is good (here, the study region is the glacierized zone), the two methods will yield similar results. Therefore, we argue that the traditional leakage has been covered by our uncertainty estimation in an untraditional way.

Finally, you may be concerned about other hydrological signals outside the region used for the EOF analysis (e.g., groundwater depletion in northern India). As I explained in my last reply to the 2nd referee, these signals are too far away to make an impact here.

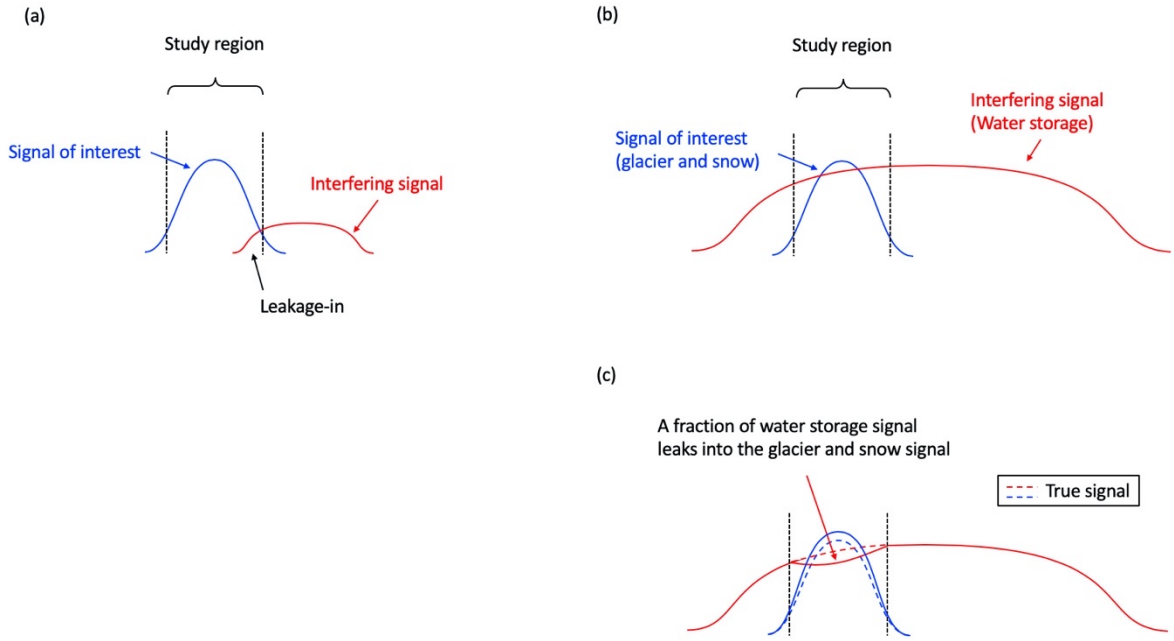

Figure R1. (a) Traditional leakage-in error. (b) Signal composition in this study. (c) A scenario when leakage occurs.

Additionally, it is not always clear which mode is used for the results in section 5. Please clarify where possible.

The GS mass estimate is solely based on the second mode. It has been clarified.

Finally, as you probably are aware, EOF analysis struggles in separating trends between different modes in physically meaningful way. When discussing the long-term trends, please include a side note discussing the glacier mass change recovered by your inversion for mode 1 and the full set of modes (i.e., the original GRACE fields).

Below are the glacier mass estimates from the second mode (yellow) and from the original GRACE fields (blue). The red curve represents the contribution of hydrological signal (the first mode) in the glacierized zone. ICESat measurements are converted into mass changes and plotted with the curves. Without the EOF decomposition of signals, the mass estimates by using GRACE cannot match the ICESat measurements in terms of either seasonal or long-term variability. Therefore, the EOF analysis can critically improve the consistency between GRACE-based GS mass estimate and those of other measurements (we discussed comparable results of ICESat and ASTER in the manuscript). This figure provides a straightforward impression of the comparative magnitude of the potential leakage from the hydrological signal if the EOF method is not used.

We have added a note in section 5.3:
The GS mass trend from the second mode is reduced by 25% compared to the original GRACE signal in the glacierized zone (Figure 4).

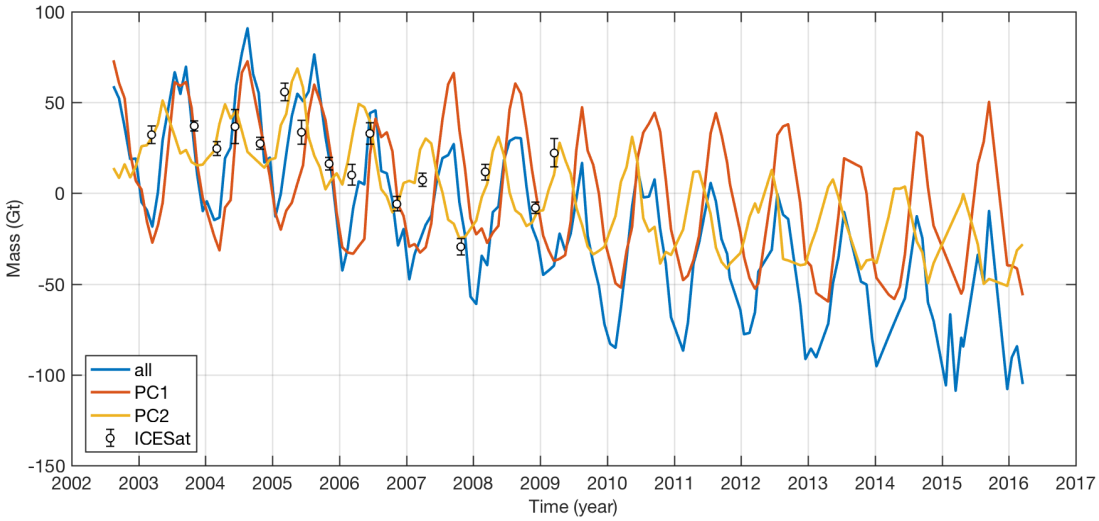

Figure R2. Mass estimate in the glacierized zone from the first two modes (PC1 and PC2) and the original GRACE time series (all).

Response to Referee #2

The authors have demonstrated ability to differentiate seasonal signal from a complex topographic region in the High Mountain Asia. It is true that the South Eastern Tibetan plateau, known as the Hengduan Shan or Eastern Himalayas experience high intensity of monsoonal precipitation (Spring and Summer), which complicates the separation of hydrological and gravity signal from GRACE satellites. General comment regarding the use of gridded precipitation products to understand the total precipitation. I feel that the authors have used less reliable precipitation data products that does not work well in the Himalayas. I would encourage the authors to use ERA5 or better products that will work for this region.

We have replaced the precipitation data HAR with ERA5, which does present the spring precipitation better. Fig. 2, Fig. S5 and Section 2.4 have been updated. However, we do not change the comparison of various datasets in the first mode of EOF analysis, since the result of TRMM outperforms that of ERA5 a bit. The comparison of the PC series is given below (corresponding to Fig. 5 in the manuscript). These two precipitation results are similar, but TRMM agrees slightly better with GRACE and NOAH (e.g., in the black dashed circles).

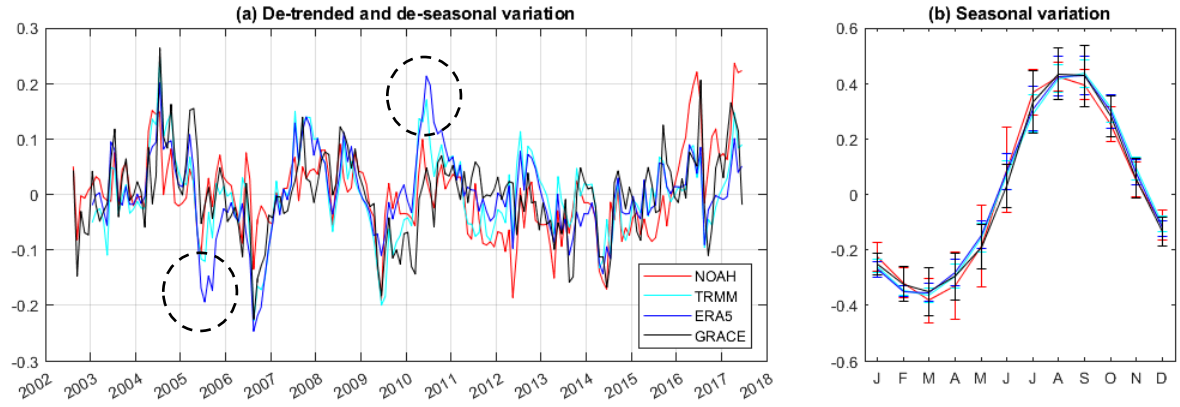

Minor comments.

1. Line 89, the authors mention the use of scale factor to compute the total meltwater contribution from river Brahmaputra. Can you explain the significance of the values used in the scale factor.

The values are explained in the previous sentence. The numerator of 0.85 represents that only 85% of the total meltwater is located in the Brahmaputra basin. The denominator of 0.83 represents that only 83% of glacierized zone is covered in the inversion. The scale factor is also explained in Section 5.3:

In our study region, 85% of its meltwater (estimated according to the area proportion) runs into the Brahmaputra and this area accounts for 83% of total glaciers in this basin (9,912 km2). Assuming that the unobserved 17% of glaciers hold the similar rate of GS mass change, our estimate of mass change is scaled by a ratio of 1×0.85/0.83=1.02 to represent the GS mass change of the entire Brahmaputra Basin.

2. Line 155: The author has mentioned 'The gridded data is compared with station observations and the correlation index ranges from 0.69 to 0.82 in the interannual variation (Figure S6), indicating a good consistency. The figure S6 indicates the recovered mass changes from the second EOF for different dataset. Can you include the corresponding figure as in the statement.

I am sorry I do not find such a problem in the supporting material. A screenshot is attached below. I guess you might download an older version.

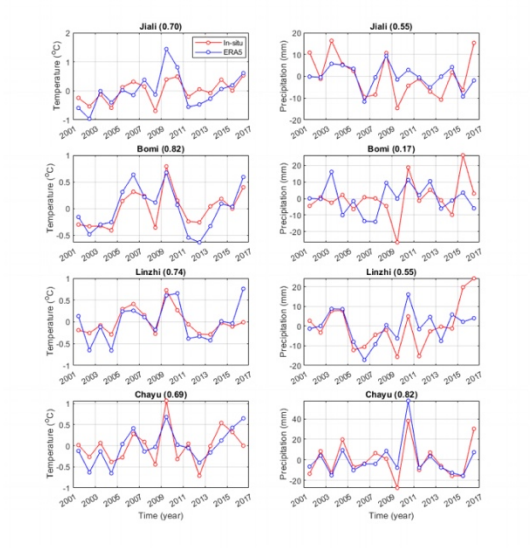

Figure S6. Comparison of annual temperature (left) and precipitation (right) records from ERA5 and in-situ observations. The correlation coefficient is given in the title. The mean value of the whole period is removed so only anomalies are shown here.

3. Line 163: Can you indicate where the localized spring precipitation is studied. Please can you remove the word 'shown later' and include the reference to a figure.

The spring precipitation covers the whole studied glacierized area. The annotation in the bracket tries to explain why a global precipitation product works poorly here. It's changed to 'Section 3'.

4. Line 200: Instead of the text 'demonstrate it later', can you include a reference to the section or figure where the peaks in three-month window offset has been noticed in the annual oscillations.

It has been changed to "Section 4.4"

5. Figure 3. Title of the figure. The white dots represent the glaciers. I assume that they are not dots, it is shaded region. The authors are requested to refer glaciers (white) as shaded regions in the rest of the figures.

Thanks for the advice. We have made such changes in the caption of Fig. 2, 3 and 4.

6. Supplement Fig S3: Instead of the word 'blue dots', can you use the words 'blue shaded region' for glaciers.

The changes have been made.

Response to Referee #3

Some of my major concerns are not addressed. I elaborate them as follows.

R0: My initial concern was not that "a sinusoidal function is unsuitable for glacier and snow mass change." I was questioning the logic of testing the orthogonality of the EOFs (Section 4.4). Please see my comments below.

R1: The analysis starts with an EOF decomposition of the GRACE data (section 4.1); two EOFs are obtained. The authors point out the hypothesis: The two EOFs separate the hydrological and glacier/snow components.

To test this hypothesis, the key is to use independent evidence to address the physical meaning of the two EOFs. An analysis of the orthogonality of the EOFs does not help (Lines 255-260 in the manuscript along with Section 3 in the supplement). The orthogonality is automatically ensured by the algebra of an EOF decomposition. The authors can always apply an EOF decomposition to the GRACE data, and the resulting basis functions will always be orthogonal, but they do not necessarily represent the hydrological and glacier/snow components. I hope this clarifies my concerns and I believe the orthogonality test should be excluded from the manuscript.

I feel there is some misunderstanding here.
> *The authors can always apply an EOF decomposition to the GRACE data, and the resulting basis functions will always be orthogonal*
I agree with you on this point, but we did not use "the resulting basis functions" in the simulation work. The glacier and snow signal was spatially generated based on the glacierized zone and was temporally varied in months. Therefore, the orthogonality is not guaranteed. As shown in the supporting material, the orthogonality is poor in many scenarios.

Why did we need this simulation work? First, we need to confirm that the inversion result is unique by carrying out the forward modeling. From the EOF result, we got two series with the peak in May and August, respectively. The August one representing the hydrological signal is easily corroborated by other datasets, but the May one representing the glacier and snow signal is hard to justify. It is possible that the glacier and snow signal actually peaks in April, but our method artificially forced it into May due to the orthogonality of the EOF approach. Without the forward simulation we could not rule out this possibility. We demonstrated in the simulation work that this possibility does not exist, so there is no multi-cause of the result.

Second, during the simulation work we found a good indicator of the leakage effect between the first two modes. The spatial pattern of the first mode is very sensitive to the leakage, which means we can quantify the leakage effect based on the smoothness of the spatial pattern.

I hope I have clarified the necessity of the forward simulation work.

R2: The response is a bit confusing. The soil moisture (SM) data employed in the manuscript are not actual observations. Is SM better represented in the model than the other water storage components (so these other components are excluded from the analysis)? I think this should be clarified.

In this region, the total water storage mainly consists of three components:
Total water storage = Soil moisture + rivers + groundwater.

Due to different replenishment rates, these three components contribute differently at different time scales. Roughly speaking, the river component is important at the seasonal scale, and the groundwater component is important at the long-term scale, and the soil moisture component is important at both scales.
The water storage in rivers is difficult to estimate due to the changeable boundaries of the braided river, and the groundwater storage is also difficult due to its invisibility. We have added an explanation in section 2.4:

The total water storage in this region also contains contributions from rivers and groundwater, which are however difficult to obtain, so only the soil moisture component is investigated here.

Fig. 3b and Fig. 5c show a clear difference in terms of spatial pattern, not just in magnitude. As I pointed out in the initial comment, Fig. 3b might be influenced by a combination of water demand from irrigation and a decrease in precipitation. These factors can affect both the magnitude and the spatial pattern, and it is likely that

these factors are embedded in the trends. For this reason, I think it would be of interest to perform the EOF analysis on the de-trended data and check if there is any improvement of agreement in the spatial pattern.

The first mode of EOF decomposition of original and de-trended results for GRACE and GLDAS datasets is shown below. The de-trending process slightly reduce the amplitude of GRACE's EOF1, but the pattern mostly remains. I guess your main concern is the location of the peak value–GRACE's EOF1 has a peak at longitude 92, while GLDAS's EOF1 has a peak at longitude 94. The main stream of Brahmaputra is at longitude 90, so the peak center in the GRACE signal shifts westward.

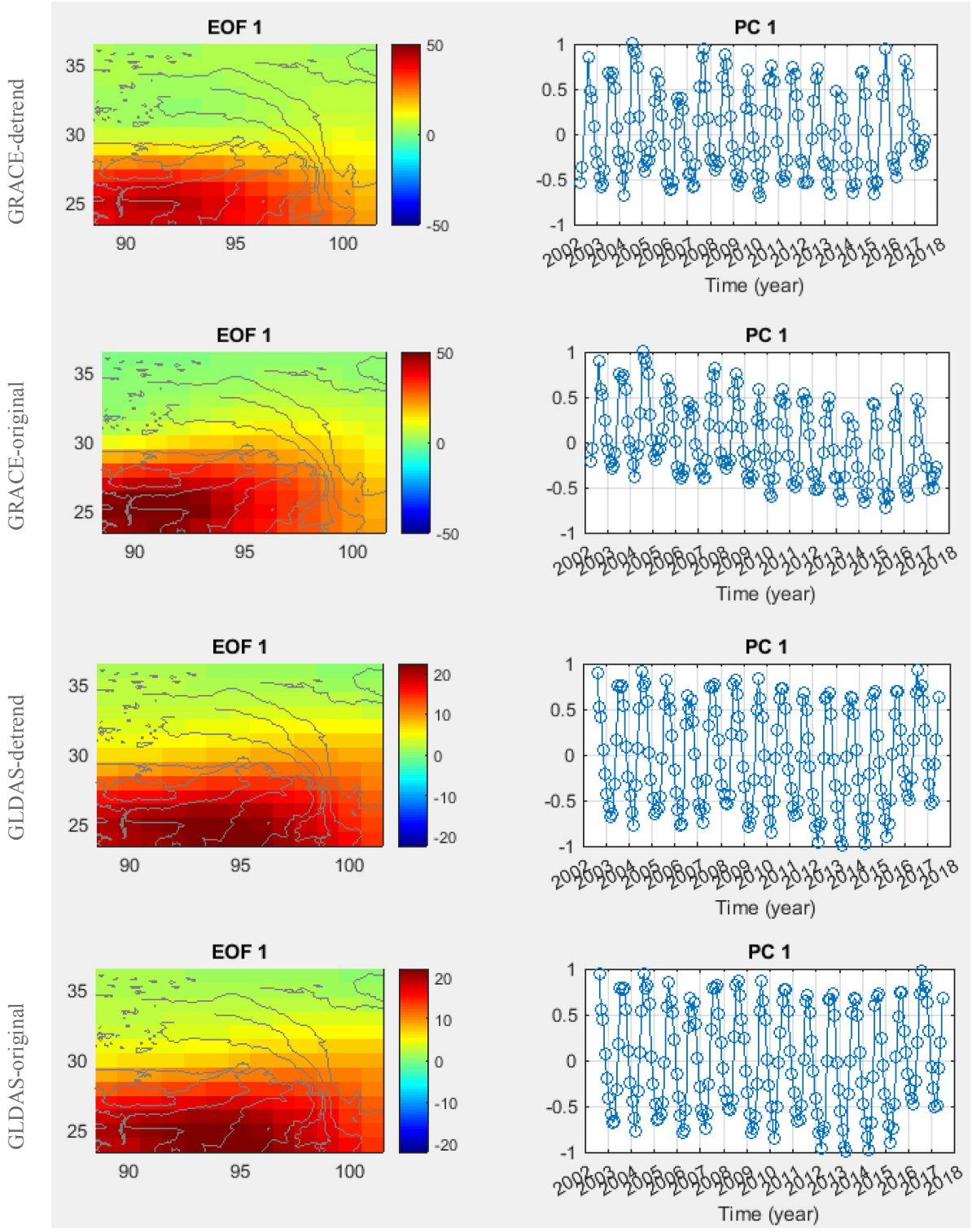

R6: Different colors in the plot represent different precipitation estimates (station, HAR, TRMM), correct? There is a big spread among these different precipitation estimates. How consistent are the EOFs from these different precipitation products?

> Different colors in the plot represent different precipitation estimates (station, HAR, TRMM), correct?
Yes. Please note that HAR is replaced by ERA5 precipitation product in the revision.

> There is a big spread among these different precipitation estimates.
The big spread is caused by the unstable seasonality in this region and it does not represent the data quality (which is difficult to quantify).

> EOFs of different precipitation products.
Below is the EOF1 of TRMM, ERA5 and GPCP (HAR is not presented due to its limited spatial coverage). The time span is August 2002–June 2017 for all datasets. The unit is mm. Note the raw datasets have been converted to have a spatial resolution of GRACE.

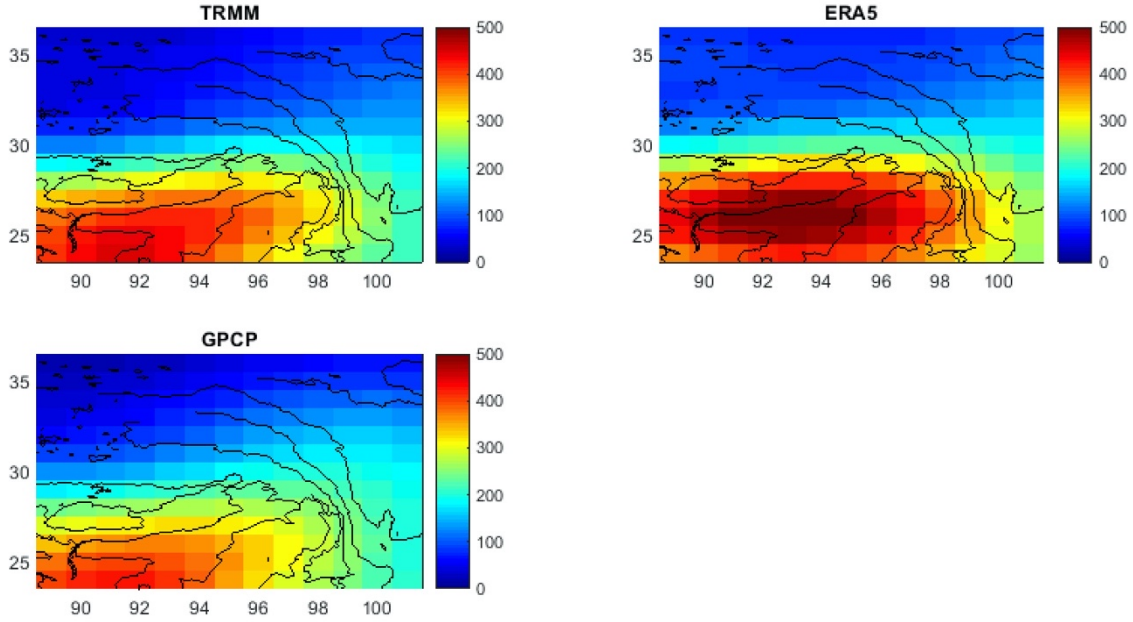

R7: Please clarify how sensitive your results are to the choice of masks.

Below are four tests of different choices of masks. Colored blocks indicate the shape of the mask, and the total area and mass inversion result are given in the title. The total area of the mask varies from 126,234 km^2 to 322,212 km^2, and the total mass estimate varies from 86.43 Gt to 89.11 Gt. The choice of mask greatly impacts the shape of the mass inversion (the mass will be more concentrated in a smaller mask), but we are only concerned with the amount of total mass, since it is much better constrained by GRACE. This insensitivity of total mass to the choice of mask is to be expected given that these masks are mostly indistinguishable under GRACE's spatial resolution.

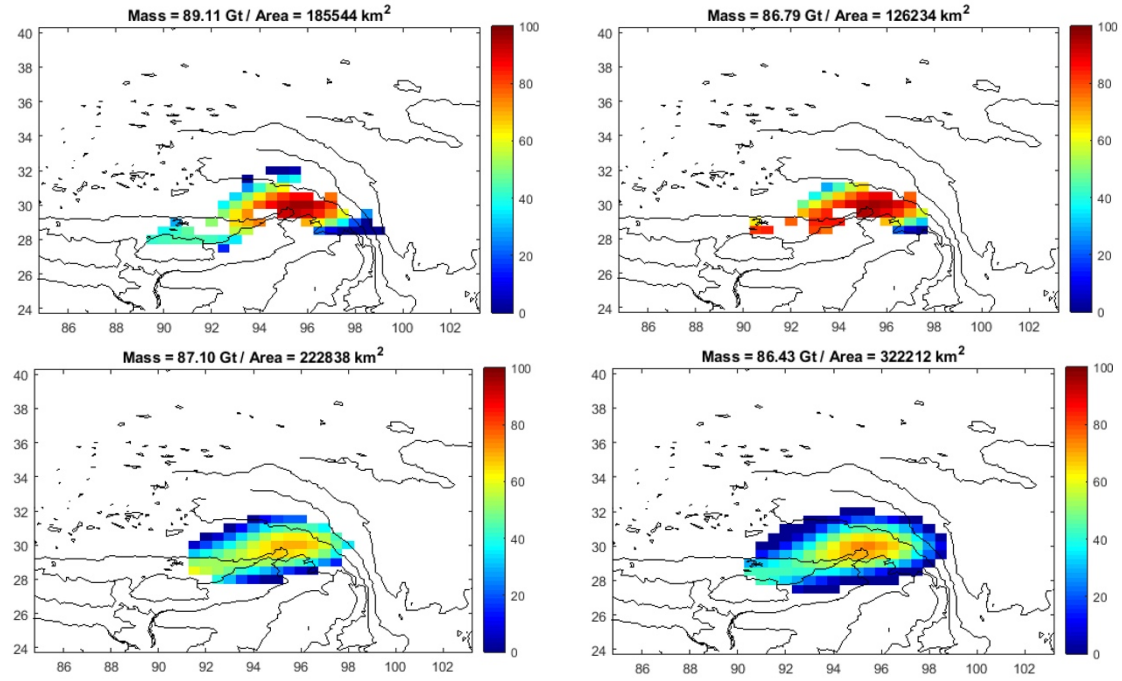

R17: Please clarify the physical basis of this weighting procedure.

The water storage change is influenced by precipitation in six months preceding the time epoch with gradually increasing weights, i.e., the closer month has a greater impact.

Track changes of manuscript

Satellite-observed monthly glacier and snow mass changes in Southeast Tibet: implication for substantial meltwater contribution to the Brahmaputra

Shuang Yi[1, 2, *], Chunqiao Song[3], Kosuke Heki[2], Shichang Kang[4], Qiuyu Wang[5], Le Chang[5]
[1]Institute of Geodesy, University of Stuttgart, 70174 Stuttgart, Germany
[2]Department of Earth and Planetary Sciences, Hokkaido University, Sapporo, Japan
[3]Key Laboratory of Watershed Geographic Sciences, Nanjing Institute of Geography and Limnology, Chinese Academy of Sciences, Nanjing, 210008, China.
[4]State Key Laboratory of Cryospheric Sciences, Cold and Arid Regions Environmental and Engineering Research Institute, Chinese Academy of Sciences, Lanzhou 730000, China
[5]Key Laboratory of Computational Geodynamics, University of Chinese Academy of Sciences, Beijing 100049, China;

Correspondence to: Shuang Yi (shuangyi.geo@gmail.com)

Abstract. High Asia glaciers ~~were~~ have been observed to be retreating the fastest in the southeastern Tibet Plateau (SETP), where vast amounts of glacier and snow (GS) feed the streamflow of the Brahmaputra, a transboundary river linking the world's two most populous countries China and India. However, the low temporal resolutions in previous observations of GS mass balance obscured the seasonal accumulation/ablation variations, and their modelling estimates were divergent. Here we use monthly satellite gravimetry observations from August 2002 to June 2017 to estimate GS mass variation in the SETP. We find that the "spring-accumulation type" glaciers and snow in the SETP reach their maximum in May. This is in stark contrast to seasonal variations in terrestrial water storage, which is controlled by summer precipitation and reaches the maximum in August. These two seasonal variations are mutually orthogonal and can be easily separated in time-variable gravity observations. Our GS mass balance ~~-~~results show a long-term trend of -6.5 ± 0.8 Gt yr^{-1} (or 0.67 ± 0.08 w.e. m/yr) and annual mass decreases ranging from ~~-43.4~~-49.3 Gt to -78.3~~-73.1~~ Gt with an average of -64.5 ± 8.9~~-57.6~~ Gt in the SETP between August 2002 and June 2017. The contribution of summer meltwater to the Brahmaputra streamflow is estimated to be 51 ± 9 Gt. This result could help to resolve previous divergent modelling estimates and underlines the importance of meltwater to the Brahmaputra streamflow. The high sensitivity between GS melting and temperature on both annual and monthly scales suggests that the Brahmaputra will suffer from not only changes in total annual discharge, but also an earlier runoff peak due to the ongoing global warming.

1 Introduction

The Tibetan Plateau, considered as the Asian water tower, is the source of several major river systems. Their upper streams are fed by rainfall, base flow and widespread glaciers and snow (GS) melt (Barnett et al., 2005; Immerzeel et al., 2010; Jansson et al., 2003; Lutz et al., 2014). The GS melt is susceptible to climate change, whereas its sustainable supply is critical to the local freshwater security, flood prevention and control, and hydroelectric development (Bolch et al., 2012; Kaser et al., 2010; Yao et al., 2012). The southeastern Tibet Plateau (SETP), including the Nyenchen Tonglha Mountains (NTM) and eastern Himalayas, holds 10,439 glaciers with a total area of 9,679 km^2 (RGI Consortium, 2017) and widespread seasonal snow coverage of up to 100,000 km^2.

These maritime glaciers are characterized by low equilibrium-line altitudes with large topographic gradients (Yao et al., 2012) and the most severe mass loss in High Mountain Asia (HMA) (Brun et al., 2017; Kääb et al., 2015). The GS melt serves as an essential water supplier for the Brahmaputra river system (e.g., Immerzeel et al., 2010; Lutz et al., 2014), which runs through three densely populated countries, China, India and Bangladesh (Figure 1). The revealed vulnerability of glaciers in the Brahmaputra Basin to global warming and emerging controversies over water allocation (e.g., dam building (Tanck and Fazani, 2010)) are increasingly attracting scientific and public concerns.

Due to the lack of observational data, most of the previous estimates on the contribution of seasonal meltwater to the upstream flow of the Brahmaputra River were based on modelling approaches that were only calibrated by employing streamflow data. ~~Resultingly~~As a result, the previous estimates disagree widely from 19% to 35% (Table 1) due to different forcing data and approaches without direct constraints on GS mass balance (Bookhagen and Burbank, 2010; Chen et al., 2017; Huss et al., 2017; Immerzeel et al., 2010; Lutz et al., 2014; Zhang et al., 2013). The amount of meltwater could be even more divergent. For example, Huss et al. (2017) estimated that the amount of annual GS melt to the Brahmaputra River was 138 w.e. (water equivalent) $km^3\ yr^{-1}$, which is however triple the estimate of 43 w.e. $km^3\ yr^{-1}$ by Lutz et al. (2014). Although these two studies covered different ranges, the glacierized zone in the basin was both well enclosed so the estimates should not be so different. Such huge discrepancies in previous estimates make it imperative to incorporate the calibration from GS mass balance observations into future modelling experiments. ~~Actually~~Recently, the concept of assimilating more GS observations has begun to be implemented in the state-of-the-art models (Wijngaard et al., 2017; Biemans et al., 2019), but their glacier results suffered from coarse temporal resolution (two observations over 5 years) and the snow mass changes were partially constrained by area changes.

Spaceborne sensors can be helpful in this desolate mountain region. Remote sensing techniques for region-wide GS mass balance measurements can be divided into three categories: laser altimetry (e.g., Ice, Cloud and land Elevation Satellite (ICESat) (Kääb et al., 2012)), multi-temporal digital elevation models (e.g., SPOT (Gardelle et al., 2013), ASTER (Brun et al., 2017)), and space gravimetry (Gravity Recovery and Climate Experiment (GRACE) (Matsuo and Heki, 2010; Yi and Sun, 2014)). The first two geodetic approaches require the average ice density to convert volume changes into mass changes. The ICESat observation suffers from short operation period (2003–2009) and sparse spatial sampling, both of which can be overcome by the stereo-imagery approach, which is becoming popular for the whole HMA study recently (Brun et al., 2017; Dehecq et al., 2018). Brun et al. (2017) provided an estimate of the detailed glacier mass balance trends over HMA between 2000 and 2016 and highlighted the regional dissimilarity. Despite recent improvements in spatial resolution in HMA glacier mass change studies, there has been little advance in their temporal resolution.

Observations at a monthly temporal resolution are necessary to separately quantify summer and winter mass balances, two processes dominating the annual glacier mass balance (Cogley et al., 2011), and thus crucial for the calibration and validation of glaciological models. The amplitude of seasonal variation of the glaciers in the SETP is up to ~3 m w.e. (Wang et al., 2017), far exceeding their net annual change of ~ 0.6 m w.e. (Brun et al., 2017). Hence, the long-term trend of GS mass changes only reflects a small net imbalance of their ablation and accumulation. ~~High time-resolution m~~Monthly observations by GRACE since its launch in 2002 (Tapley et al., 2004) are promising in identifying these two processes. Up to now, the application of GRACE in HMA glaciers has been focusing on their secular changes with little attention to the seasonal variations (Gardner et al., 2013;

Matsuo and Heki, 2010; Yi and Sun, 2014). This is mostly due to the poor spatial resolution of GRACE (> 300 km) and the dominance of terrestrial hydrological signals in the seasonal gravity signals, which is difficult to eliminate from glacial signals. The latter is particularly severe in the SETP with intense monsoon precipitations. The GS and hydrological mass changes (mainly including mass changes in rivers, soil moisture and groundwater) dominate the seasonal gravity signals in the SETP observed by GRACE. Despite the general difficulty in separating them in the spatial domain, we find it possible to separate the two signals in the time domain, owing to their contrasting seasonal behaviours.

Precipitation in the SETP is controlled by various atmospheric circulation systems in different seasons, with westerly winds and Bay of Bengal vortex in winter/spring and Indian monsoon in summer (Wu et al., 2011; Yang et al., 2013; Yao et al., 2012). The former two systems were found to drive the spring precipitation in the SETP along the Brahmaputra River, thus forming a 'spring-accumulation' type of glaciers (Yang et al., 2013). The Indian monsoon prevails from June to September and brings intense precipitation on the southern side of the Himalayas, where terrestrial water storage shows tremendous seasonal changes and peaks in late summer. Therefore, according to the climate stations near NTM, we can observe bimodal precipitation variations throughout the year (Yang et al., 2013).

In this work, we will first introduce the precipitation characteristics in this region by both meteorological stations and global precipitation products. We will then use the empirical orthogonal function (EOF) analysis to decompose hydrological and GS signals in our study region, which does not exactly coincide with the range of glacierized zone in the Brahmaputra Basin. Our study region covers only 83% of the basin glaciers (the 17% undetected ones are in the western part) and 15% of non-Brahmaputra glaciers. We will scale our results by a ratio of $1 \times \frac{0.85}{0.83} = 1.02$ to get the total meltwater in the Brahmaputra, assuming that our observations can represent the basin-wide average. The hydrological and GS signals are further compared to the results of other datasets to validate their physical meanings. Such high time-resolution observations also allow us to compare GS mass variations with temperature records during the ablation season, and to study the sensitivity of GS mass change in response to the temperature change. Finally, we will compare our results to previous estimates at monthly, annual, and interannual scales.

2 Data

2.1 GRACE data and preprocessing

We adopt the monthly GRACE spherical harmonics Release 06 products from August 2002 to June 2017. The three datasets are solved respectively by three organizations: Center for Space Research (CSR) at the University of Texas, GeoForschungsZentrum (GFZ) in Potsdam, and the Jet Propulsion Laboratory (JPL). These datasets are available at ftp://podaac.jpl.nasa.gov/allData/grace/L2/. The degree 1 terms, which are absent in original GRACE releases, have been added based on the technique proposed by Swenson et al. (2008). The C_{20} terms have been replaced by those from satellite laser ranging (Cheng et al., 2011), which are considered to be more reliable. A widely used Glacial Isostatic Adjustment (GIA) model by A et al. (2013) is adopted to correct the GIA effect caused by historical polar ice sheet changes.

Two different filtering strategies, a combination of P4M6 decorrelation (Swenson and Wahr, 2006) and 300km Gaussian filter (hereafter short for G300+P4M6) and a DDK4 filter (Kusche et al., 2009), are applied

separately. Therefore, there are six combinations and their average values (with uniform weights) are used in the following figures.

2.2 GRACE error estimation

We adopt different uncertainty estimation strategies for the seasonal variation and the trend due to their intrinsically different error sources. The error of seasonal variation consists of the standard deviations among these six datasets (i.e., errors from the data solution and smoothing methods) and the leakage error, while that of the long-term trend also includes other potentially uncorrected signals. The leakage error is determined by how effectively the hydrological and ~~glacial~~ GS signals are separated by the EOF technique. Based on the modelled and recovered glacier mass changes, their residuals are estimated to have a seasonal variation of up to 11% of the modelled glacier mass change (refer to section 3.2 in the supporting materials), which is used to calculate the seasonal leakage error.

For the long-term trend error, the three different solutions and two smoothing techniques have a total effect of 0.44 Gt/yr. There are potential errors from other signal sources, like glacial isostatic adjustment (GIA), Little Ice Age~~little ice age~~ (LIA) and weather denudation. The GIA effect which originates from the polar regions has been corrected by A's GIA model (A et al., 2013), although its influence on the trend is as small as 0.02 Gt/yr. The main reason is that the spatial pattern of GIA is quite smooth, so it mainly influences the first mode and rarely leaks into the second one. This feature is also applicable for other signal sources: unless they exactly locate in the glacierized area, their influence will be reduced by the EOF decomposition. In the southern and southeastern Tibetan Plateau (over 500,000 km^2), the effects of LIA and denudation are estimated to be -1 ± 1 Gt/yr (Jacob et al., 2012) and 1.6 Gt/yr (assuming the sediment has a density of 2 Gt/km^3) (Sun et al., 2009), respectively. Our glacierized zone and surroundings have an area of about 100,000 km^2, accounting for one-fifth of the whole region, so we suppose their contribution to the GS mass estimate is also proportionally 1/5. However, as we explain above, we could not precisely quantify their contribution without knowing their spatial distribution, and they are more likely to be absorbed by the first mode, so we only include their contribution in the error estimation rather than correcting them in the trend. Table 2 summarizes the sum of GRACE error estimates in the secular trend.

2.3 ICESat altimetry

Version 34 of the ICESat Global Land Surface Altimetry Data is used to derive glacier height changes. The data span is from 2003 to 2009, with two or three observation campaigns per year (Figure S1). The processing of ICESat data includes the following steps. (1) Orthometric heights are obtained from original elevation data based on the Earth's gravity model 2008. (2) Footprints on glaciers are identified based on RGI 6.0 glacier outlines. (3) For each ICESat footprint, SRTM (Farr et al., 2007) elevations and slopes are extracted by bilinear interpolation of the DEM grid cells. Glacier height variation is defined as the elevation differences between the footprints and the SRTM data. (4) We exclude footprints over SRTM voids, footprints with slopes higher than 30°, and footprints with height change larger than 100 m (which are attributed to biases caused by cloud cover during the ICESat acquisition). (5) We also discard the calibration campaign L1AB (March 2003) and the incomplete campaign L2F (October 2009). (6) Glacier height variations are averaged and interpolated along the altitude to alleviate the

uneven sampling problem in space, and an uncertainty of 0.06 m/yr (Kääb et al., 2012) is chosen to account for the uneven sampling bias in time. The steps have been used in previous work (Wang et al., 2017) and have also been described in earlier studies (Gardner et al., 2013; Kääb et al., 2012). The footprint information is given in Figure S2.

ICESat has shown good ability to solve snow variation in flat regions (Treichler and Kääb, 2017), but applying the same technique in mountainous areas with high terrain heterogeneity is cumbersome. Therefore, here ICESat is only used to estimate changes in glacier mass. Although our GRACE estimate includes both glaciers and snow, the estimates by GRACE and ICESat are comparable in the late ablation season (i.e., the October/November campaign of ICESat), when the contribution of seasonal snow meltwater is negligible (Section 5.1). To convert the glacier thickness changes into mass changes, two parameters are required, i.e., glacier density and total glacier areas. We assume an average glacier density of 850 ± 60 kg m^{-3} (Huss, 2013). According to the glacier inventory RGI 6.0 (RGI Consortium, 2017), the area has a glacierized area of 9,679 km^2.

2.4 Other auxiliary data

To analyse the impact of temperature and precipitation on GS and water mass balance here, we adopt two types of datasets, the gridded reanalysis products and in-situ measurements from four meteorological stations (their locations are labelled in Figure 1, and coordinates are listed in Table S1). Precipitation and temperature records for each site from 2003 to 2016 (Figure S4) are available from the China Meteorological Data Service Center (http://data.cma.cn/data/weatherBk.html). Only four in-situ temperature records may not represent the overall condition of the glacierized zone, so we adopt the gridded temperature product from the ERA5 reanalysis data processed by the European Centre for Medium-Range Weather Forecasts (ECMWF). The data is available at https://www.ecmwf.int/en/forecasts/datasets/reanalysis-datasets/era5. The gridded data is compared with station observations and the correlation index ranges from 0.69 to 0.82 in the interannual variation (Figure S6), indicating a good consistency. The average values in the glacierized zone from the ERA5 temperature product will be used to represent the temperature condition here.

Global gridded precipitation data Tropical Rainfall Measuring Mission (TRMM) (Huffman et al., 2014) is used to examine the influence of precipitation on water storage. The data is available at https://pmm.nasa.gov/data-access/downloads/trmm. Although such a global product is unable to capture the localized spring precipitation in our study area (Section 3), it can be used for the investigation of large-scale monsoon precipitation. ~~We also use High Asia Refined analysis (HAR) precipitation product generated using the atmospheric model WRF (Maussion et al., 2014). In this product, long-term precipitation trends are not recommended, but its 10 km spatial resolved seasonal variation is informative to investigate the spatial extent of spring precipitation. The HAR data is available at http://www.klima-ds.tu-berlin.de/har/.~~

Moderate-resolution imaging spectroradiometer (MODIS) data MOD10 (Hall et al., 2006) is used to investigate snow coverage here. The MOD10CM product has a temporal resolution of 1 month and spatial resolution of 0.05-degree. The land surface model Global Land Data Assimilation System (GLDAS)-NOAH (Rodell et al., 2004) is adopted to inspect soil moisture changes, which can be compared to changes in total terrestrial water storage estimated by GRACE. Here, the version 2.1 monthly product with 1.0-degree spatial resolution is used (available at https://hydro1.gesdisc.eosdis.nasa.gov/data/GLDAS/GLDAS_NOAH10_M.2.1/). The total water storage in

this region also contains contributions from rivers and groundwater, which are however difficult to obtain, so only the soil moisture component is investigated here.

3 Spring precipitation and mass increase

The method of this study is based on the fact that the change in GS mass driven by spring precipitation precedes the change in hydrological signals. Therefore, before introducing the method, we want to demonstrate that GRACE can detect mass changes caused by spring precipitation. At two out of four stations (Bomi and Chayu), spring precipitation is noticeable, even surpassing the summer/autumn precipitation brought by the Indian monsoon (Figure S4). Yang et al. (2013) provided precipitation records at 22 sites in a broader area and outlined the boundary of the impact zone of the spring precipitation, which roughly covers the glacierized area studied here. Summer precipitation and its associated hydrological mass change are enormous and well recognized, while the spring one is not. Therefore, here we only use the TRMM and ~~HAR~~ ERA5 results from January to March in Figure 2 to show the initiation of spring precipitation. The precipitation begins to spread south and west ~~since~~ starting April, when the monsoon gradually increases (not shown here). The TRMM results show a boundary along the latitude 29° N, where the precipitation suddenly decreases to the north. This boundary of change is irrelevant to the terrain and seems to be artificial. This phenomenon cannot be found in the ~~HAR~~ ERA5 result, which shows abundant precipitation in the glacierized zone in these months. The bottom plots give the GRACE monthly mass anomalies from March to May (two months later than the precipitation), ~~because we found such a time lag in the response of mass change to precipitation~~as GRACE observes the cumulative mass change resulting from precipitation. An earlier mass increase from April can be identified in the southeastern part of the Tibetan Plateau.

The performance of TRMM and ~~HAR~~ ERA5 is compared with our station measurements in Figure S5. According to the in-situ records, the spring precipitation, as a part of the bimodal variation, is obvious at the Bomi and Chayu stations. TRMM is capable of revealing the condition at Chaya at 28.65° N, but performs poorly in regions north of 29° N. The ~~HAR~~ ERA5 data ~~,~~ demonstrates a higher precipitation in winter and spring at Bomi and Linzhi than the other two datasets.~~seems to slightly underestimate the precipitation in April but overestimate in Autumn and Winter, and thus does not present a clear bimodal change.~~

These results show that spring precipitation can be captured to a limited extent by various reanalysis products and the 'spring-accumulation' pattern of GS mass change in the SETP is recognizable in GRACE observations. The amplitude and phase of the seasonal mass variation from the equivalent water height (EWH) of GRACE are compared in the background of Figure 1. The seasonal amplitude has a spatial distribution similar to that of the Indian monsoon affected area. This pattern reflects the predominance of the monsoon-controlled hydrological process and the weaker glacial signals in this region. However, the peak month of seasonal changes (the contours in Figure 1) divergently appears earliest in June in the NTM and gradually delays to August in the southern Himalayas, where the annual amplitude reaches its maximum. The shift in peak months reflects the increasing/decreasing contribution from the sinusoid of the hydrological/GS seasonal variation. A key point to point out is that their peaks have a three-month time window offset (Section 4.4), which is a quarter of the annual oscillation cycle and means that the two signals are mathematically orthogonal.

4 Decomposition of GRACE signals

4.1 EOF analysis of GRACE

GS and hydrological mass changes dominate the seasonal gravity signals observed by GRACE in this region and they are mathematically orthogonal due to different phases. Therefore, we employ the EOF technique (see the supporting material for mathematic expressions) (Björnsson and Venegas, 1997) to decompose hydrological and glacial signals in the GRACE datasets (**Figure 3**). We thus extract two modes with significantly higher explained variances than the other modes (i.e., two significant modes are obtained). Results of different datasets and filters show good consistency, indicating that the first two modes are robust.

Each mode consists of one EOF (the spatial pattern) and one PC (the temporal evolution). Only the first two modes, respectively accounting for 79 ± 5% and 12 ± 4% of the total variance explanation, are shown. Although the first mode is much stronger than the second mode (because the second one is more localized), their signal strength in the glacierized region is comparable on both seasonal and secular temporal scales. Modes above 2 are weak and irregularly show much noise, so they are discarded here.

The trends of the GRACE observation and its decomposed modes are shown in **Figure 4**. The GRACE observation shows a significant mass loss, which is divided into the first two modes. In the glacierized zone, ~ 2/3 of the negative trend comes from the 2nd mode and ~1/3 comes from the 1st mode. The trend of higher modes (> 2) is quite weak (**Figure 4**d).

According to the spatial coverages (EOF_1 and EOF_2) and their temporal variations (PC_1 and PC_2), the first mode covering the low altitude areas on the south of the plateau with a peak month in August/September seemingly represents hydrologic signals and the second mode concentrating in the glacierized region with a peak month in May (the peak month of June in Figure 1 is the mixed result of the first two modes) seemingly represents glaciers. We will verify these hypotheses below.

4.2 GS mass estimation from mode 2

GRACE results only show smooth mass patterns and we need some strategy to recover the original amount of mass changes. If we adopt the second mode to estimate GS mass change, this step is necessary. Therefore, a forward modelling method (Yi et al., 2016) is chosen to recover the mass in a pre-defined region iteratively. This method has been widely used (Chen et al., 2015; Wouters et al., 2008), especially in the study of polar ice sheets. In the first step, we divide the glacier mask based on the glacier distribution recorded in RGI 6.0 (RGI Consortium, 2017) (Figure 4e). The lattices have a resolution of 0.5° by 0.5° and are located in glacierized area (by this way we assume the snow signal also comes from the glacierized area, but it does not influence the total mass estimates). In the second step, the mass in each lattice is iteratively adjusted until its smoothing signal (Figure 4f) ~~well~~ matches the GRACE observation (Figure 4c) and becomes stable. The details of each combination of datasets and filters are presented in Figure S7 and S8. Therefore, we solve the mass in each combination (Figure S8). The mass is multiplied by the PC_2 series to derive the glacier mass series, and their average is taken as the mass estimate, which will be compared with ICESat observations to test our hypothesis on its physical meaning.

4.3 Validation of mode 1 by soil moisture and precipitation datasets

To validate the hypothesis that the first mode represents hydrological signals, we compare it with EOF decomposition results of two other datasets, soil moisture from GLDAS/NOAH and precipitation data from TRMM (Figure 5). To make them comparable to GRACE in terms of spatial resolution, they are expanded into spherical harmonics, truncated at degree 60, and smoothed by the same filter. Their results are shown in Figure 5. Different from GRACE that has two significant modes, they only have one due to the lack of a glacial signal. The EOF_1 of GLDAS/NOAH and TRMM is consistent with that of GRACE. The PCs are compared at interannual and seasonal scales as well. Note that precipitation is an instantaneous amount, while water storage is a state value, so the former should be integrated in time to make it comparable to the latter. Here, we integrate precipitation in successive six months by an empirical weight function of (1, 2, 3, 4, 5, 6), which will be normalized, and the value is attributed to the sixth month. Different integration methods are tested in the supporting materials.

Of note, mass contributions from the Brahmaputra River and groundwater are absent (and they are troublesome to obtain) and precipitation is assumed as the dominant driver of water storage change without considering the influence of runoff and evaporation (Humphrey et al., 2016), so we do not expect that we can reach a thorough agreement between different datasets. This is acceptable if their temporal consistency is targeted. However, long-term trends in runoff, evaporation and groundwater cannot be ignored and they are differently reflected in these three products, so their trends have been removed before the comparison. The exclusion of unavailable surface water and groundwater in the GLDAS result also causes a weaker strength of its EOF_1 compared to that of GRACE. We conclude that these datasets should be comparable in terms of seasonal and interannual variations and the pattern of spatial distribution, but not in the long-term trend and the amplitude of the spatial distribution. The good resemblance in both the EOF_1 (spatial pattern) and PC_1 (seasonal and interannual temporal evolution) between GRACE, GLDAS/NOAH and TRMM indicates that they reflect similar geophysical processes, i.e., hydrological variations.

4.4 Method feasibility and reliability

The phase difference of 3 months is a prerequisite for this method and can be verified retrospectively. We tested different phase differences between hydrological and GS signals and decomposed them by the EOF method (refer to section 3.1 in the supporting material). Two conclusions are obtained: only when the GS mass change peaks in May (3 months before the peak month of the hydrological signal) can our simulated result agree with the GRACE observation; the EOF decomposition can well restore both seasonal variation and the trend of the GS signal if the orthogonality is satisfied.

Only hydrological and GS signals can explain the first two modes considering their spatial and temporal patterns. Atmosphere contribution has already been removed in GRACE observations (Dobslaw et al., 2017) and mass transports of solid earth are unlikely to have such strong seasonal variations. We cannot quantify the contribution of groundwater in the second mode, but groundwater is apt to be modulated by stronger rainfalls in summer (Andermann et al., 2012), rather than snowfalls in winter-spring, and groundwater activity will be reduced in winter-spring when the ground is frozen. Therefore, the groundwater component is inclined to ~~exist only in~~be captured by the first mode. We attribute the~~The~~ negative trend in the first mode ~~is mostly due~~ to decreasing precipitation in recent years (Figure S9) and intense groundwater pumping (Shamsudduha et al., 2012). The

negative trend in the second mode is supposed to represent GS melting and can be used for estimating GS mass balance.

5. Results and discussion

5.1 Glacier and snow mass balance

The glacier surface elevation changes measured by the ICESat are compared with ~~our GRACE based~~the result estimated from the second mode of GRACE~~s~~. We interpolate the series of GRACE estimates (2002–2017) into the observation epochs of ICESat (2003–2009) and plot mass changes by GRACE as a function of elevation changes by ICESat (Figure 6a). After ~~divided~~ dividing by the glacier density, the slope of the elevation-mass regression line represents the inventorial glacierized area by RGI 6.0. The observations in October/November (blue squares) ~~coincide~~ approximate with the line, indicating the good consistency between ICESat and GRACE in the late ablation season between 2003 and 2009. The MODIS result indicates that the snow coverage increases rapidly since September (Figure 6b), while the GRACE PC_2 series show a moderate increase after October. We speculate that the snow height does not increase much in the first few months so the contribution of snow mass is not significant. The observations in March and June, as expected, are well above the line, implying an extra snow mass contribution, which can be inferred from the point-to-line vertical distance. The snow contribution relative to the total mass anomalies varies drastically between 0% and 62% with a mean value of 38% within our observation time windows.

The difference between GRACE and ICESat-based estimates of mass change indicates that the snowpack outside the glaciers is a non-negligible contributor to the seasonal mass variation. This is quite different from previous glacier trend estimates, where non-glacier snow was neglected. Based on MODIS observations, the snow coverage area in this region varies from approximately 80,000 km^2 in winter to 30,000 km^2 in summer, both of which are much larger than the inventoried glacier area (Figure 6b). However, heterogeneous snow depths (Das and Sarwade, 2008) and densities across the vast and rugged area make it difficult to measure their mass change by a non-gravimetric way.

Figure 6c compares the time series of glacial mass in the SETP from GRACE (August 2002–June 2017) and ICESat (2003–2009). The times series from two sensors are consistent in seasonal and interannual variations, despite the absence of the snow component in the ICESat result. Monthly mass change shows that the ablation season is generally between June and October with slightly varied initiation and duration from year to year. The maximum mass increase (10–20 Gt) usually occurs in April, when the spring precipitation peaks, and the severest mass loss (-15 – -30 Gt) usually occurs in July when the temperature peaks. As the temperature rises from April to July, the monthly mass change curve drops steeply from the peak down to the trough, but the ascending process with mass accumulation is relatively moderate and continuous.

We calculate annual mass increase and decrease by the difference of mass anomalies between November and May and between June and October, respectively. From 2002 to 2017, the annual mass decrease ranged from -49.3~~3.4~~ Gt to -78.3~~3.1~~ Gt with an average of -64.5 ± 8.9~~57.6~~ Gt, and the annual mass increase ranged from 41.8~~35.7~~ Gt to 79.9~~63.4~~ Gt with an average of 58.6 ± 11.0~~50.5~~ Gt. The seasonal GS mass changes postpone the runoff of ~6~~5~~0 Gt of winter-spring solid precipitation for several months. This amount plays a vital role in the annual streamflow (130.7 Gt on average) of the upper Brahmaputra (Lutz et al., 2014) and is almost ten times the

annual net meltwater. Without the buffering effect of the seasonal variation, there will be a tremendous reduction in the streamflow in summer and autumn, when the water demand is high, and adaptive management on the dams in the Brahmaputra will be required to reduce seasonal irregularities in the streamflow (Barnett et al., 2005).

5.2 Quantifying the sensitivity of glacier and snow melt to temperature

Temperature is a dominant factor influencing the melting of glaciers (Cogley et al., 2011). Here, the monthly temperature records from the ERA5 product are compared with month-to-month mass changes by GRACE to investigate the sensitivity of the GS mass balance in response to temperature change (Figure 7). Mass changes are negatively correlated with the temperature anomalies by a factor of -1.9 ± 0.2 Gt degree^{-1} during the ablation season (from May to October) but no correlation is found during the accumulation season (from November to April). The mass peaks around May, when either glacier accumulation or ablation could happen. The temperature averaged in this transitional month is taken as the reference for the temperature anomalies used in the figure and their mass changes are annotated. The highest sensitivity of monthly mass changes in response to temperature is observed in July (3.1 ± 2.5 Gt degree^{-1}), when the largest monthly mass loss occurs.

To investigate the impact of climatic variables on the interannual variations of GS mass, we compare annual mass losses (from May to October) with summer temperatures (from June to August) (Figure 7b). The annual mass loss is significantly correlated with the summer temperature, with a slope of -10.7 ± 4.2 Gt degree^{-1} (P-value: 0.025, R^2-value: 0.35), indicating that the annual GS mass balance is sensitive to summer temperature. The small value of R^2 is partly due to the relatively large uncertainties of our mass estimate (10 Gt) in this modest range of variation (30 Gt) and the neglect of other factors influencing GS mass balance. The sensitivity index was provided by a previous study (Sakai and Fujita, 2017), where the whole HMA was examined and the SETP shows a widespread high sensitivity with an average value of -1.23 m w.e. degree^{-1}. Based on the glacierized area of 9,679 km^2, our estimation is -1.10 ± 0.43 m w.e. degree^{-1}, which is comparable with the earlier study of Sakai and Fujita (2017). It should be pointed out that annual net mass balance was used in Sakai and Fujita (2017) in comparison with the annual mass loss used in this study, although annual net mass balance is mainly driven by summer melt (Ohmura, 2011).

We could not find a significant relationship between the mass and precipitation changes, probably because our data fail to reflect the strong orographic effect in precipitation, and/or the GS mass gain process is too complex to be attributed to precipitation alone.

5.3 Comparison with previous estimations on glacier and snow meltwater

The trend of glacier elevation change by ICESat in this study is -0.65 ± 0.20 m w.e. yr^{-1} during 2003–2009, which lies between the values of -0.30 ± 0.07 m w.e. yr^{-1} (Gardner et al., 2013) and -1.34 ± 0.29 m w.e. yr^{-1} (Kääb et al., 2015) in eastern NTM by using alike ICESat dataset (but of an older version), and is close to the trend of -0.62 ± 0.23 m w.e. yr^{-1} during 2000–2016 by using ASTER (Brun et al., 2017). The trend of GS mass change in this study by using GRACE is -6.5 ± 0.8 Gt yr^{-1} between August 2002 and June 2017. The mass contribution from snow is considerable at the seasonal scale but negligible over 15 years, so the secular trend by using GRACE mainly represents the glacier mass change. Our GRACE trend consists well with the derived glacier mass change of -5.5 ± 2.2 Gt yr^{-1} by using ASTER (the area-averaged rate in NTM and Bhutan multiplied by the glacierized area of 9,679 km^2). In conclusion, both of our ICESat and GRACE estimates agree well with the previous ASTER

result in terms of secular trend. The GS mass trend from the second mode is reduced by 25% compared to the original GRACE signal in the glacierized zone (Figure 4).

A recent result on changes in interannual glacier flow in this region (Dehecq et al., 2018) indicates a strong correlation between ice flow rate and changes in glacial thickness. The interannual variation of GRACE-based mass changes (the 1-year smoothed sequence in Figure 6c) notably shows equilibrium during periods of 2003-2005 and 2011-2014. According to the ~~previous~~ aforementioned study (Dehecq et al., 2018), thinning glaciers reduce their flow rate by weakening gravitational driving stress; therefore, this balanced mass state may slow down the decreasing flow rate. Coincidentally, we can identify such decelerating phase in the decline of glacier flow rate during 2004-2006 and 2012-2015 (Figure 1 in Dehecq et al., 2018).

GS mass loss is caused by flow, melting, and evaporation processes, while the last one does not contribute to the river flow. Evaporation is important for continental-type glaciers where the climate is usually cold and dry. E.g., it accounts for 12% of the glacier ablation in Tianshan (Ohno et al., 1992). However, the importance of evaporation is greatly reduced in our maritime glaciers due to the extremely humid air and rapid melting. Therefore, we ~~suppose~~ assume that the mass loss is completely turned into meltwater and can be compared with analogous outputs from models. In our study region, 85% of its meltwater (estimated according to the area proportion) runs into the Brahmaputra and this area accounts for 83% of total glaciers in this basin (9,912 km^2). Assuming that the unobserved 17% of glaciers hold the similar rate of GS mass change, our estimate of mass change is scaled by a ratio of $1 \times 0.85/0.83 = 1.02$ to represent the GS mass change of the entire Brahmaputra Basin. Monthly changes of meltwater estimated by month-to-month difference in GRACE results are compared with model results of Lutz et al. (2014), which showed that GS melt constitutes 33% of the total discharge in the Brahmaputra and that 50% of the annual melt occurs in the summer (Figure 8). GRACE only detects the net change in GS and cannot separate mass ablation and accumulation (see the inset in Figure 8). Because these two processes concur simultaneously in transitional seasons and offset to some extent, the annual mass decrease (total mass loss in a year; here, ranges from ~~44.5~~49.3 km^3 to 78.3~~74.8~~ km^3 with an average of ~~59.0~~64.5 km^3) is smaller than the real GS melt. As a result, the annual mass decrease provides a lower bound on annual GS melt each year, rather than an accurate estimate. Instead, the amount of GS melt can be better determined during the summer (from June to August), when the accumulation is supposed to be small. This value can be used to validate the model output. Our result shows that the summer melt ranges from 37.3 km^3 to 62.9 km^3 with an average of 51.6 km^3, which is over 100% larger than the 23 km^3 GS mass change given in the model of Lutz et al. (2014) (Figure 8). Although extrapolated mass changes for the undetected 17% of glaciers and the neglected summer evaporation may reduce our estimates of summer meltwater, they definitely cannot explain the difference of more than 100%. Among all model estimates, the model of Lutz et al. (2014) reported one of the largest proportions of GS melt contribution (33%), but still largely underestimated the amount of summer meltwater, according to our estimate from satellite observations.

Our annual mass decrease (average 49.0 Gt) is still much smaller than the 137 Gt annual meltwater given by Huss et al. (2017). However, this ~~enormous~~ larger value even exceeds the annual streamflow of 130.7 km^3 in the upper Brahmaputra where all GS meltwater is included (Lutz et al., 2014). The upper streamflow at the Nuxia station (ahead of the main glacier supply area) is ~ 60 km^3. Therefore, the difference in streamflow between the main glacier supply area is ~ 70 km^3, and the annual meltwater is unlikely to exceed this value, considering the

additional contribution of precipitation. These values generally represent decadal averages at the beginning of this century (Table 1) and they are therefore comparable.

6 Conclusion

In this study, we use GRACE gravimetry to estimate the GS mass balance in the SETP from August 2002 to June 2017. The second EOF mode of GRACE observations is attributed to changes in GS mass, which can be validated in the following three steps. First, a simulation experiment shows that two signals with peaks in August and May can be decomposed unbiasedly by EOF. Second, the first decomposed mode shows consistent spatio-temporal patterns with the soil moisture and precipitation variations from the GLDAS and TRMM data and thus can be reasonably attributed to hydrological processes. Thirdly, the second mode of GRACE signal with a peak in May temporally corresponds to the glacier/snow accumulation and ablation processes and spatially coincides with the glacier distribution, which is also supported by the spring precipitation pattern observed by meteorological stations. Glacier mass change measured by ICESat is further adopted to compare with our GRACE-based GS estimates, and good agreement is reached in the ablation season when the snow contribution is negligible. The ICESat measurements also show that the seasonal glacier mass variation is large, which is consistent with our finding that GS mass change in this region peaks in May.

The GRACE-based GS mass balance not only shows a long-term decreasing trend of -6.5 ± 0.8 Gt yr^{-1}, generally comparable with previous studies on glacier mass balance in the SETP, but also newly reveals a strong seasonal variation which postpones water supply of about 60~~50~~ Gt from winter and spring to summer and autumn. The high sensitivity of glacier mass changes responding to temperature shows that warming climate will exert strong impacts on the glacier and snow mass balance from two aspects. On the one hand, under the current glacier condition, the increase in summer temperature will enhance the annual meltwater by a factor of -10.7 ± 4.2 Gt $°C^{-1}$; On the other hand, the seasonal meltwater will shift earlier and reduce its supply in summer and autumn, which is potentially ten times the amount of annual glacier melting. Our estimates of monthly GS meltwater can also give an elaborate calibration on the glacier accumulation and ablation processes in hydrological and glaciological models of the Brahmaputra Basin, which were barely calibrated by GS mass observations and diverged largely on the proportion of seasonal meltwater contribution. Given the high vulnerability to warming temperature, the greater contribution of meltwater to the Brahmaputra streamflow than most model estimates indicates that its water resource allocation will face ominous tension in the future.

Data availability

The data that support this study are mostly publicly open and their sources are indicated in the data section. The meteorological data and the series of glacier mass balance estimate are available upon request to the corresponding author.

Author contributions

S.Y. conceived the study and conducted the calculations. S.Y. and C.S. analyzed the results and wrote the manuscript. K.H. discussed and revised the manuscript. S.K. discussed and suggested the experiment. Q.W. processed the ICESat data. L.C. processed the MODIS data.

Competing financial interest

The authors declare no competing financial interests.

Acknowledgments

S.Y. is supported by JSPS KAKENHI Grant Number JP16F16328 and the Alexander von Humboldt Foundation. C.S. is supported by the Strategic Priority Research Program of the Chinese Academy of Sciences (grant no. XDA23100102) and the National Key R and D Program of China (grant no. 2018YFD1100101, 2018YFD0900804)

References

A, G., Wahr, J., and Zhong, S.: Computations of the viscoelastic response of a 3-D compressible Earth to surface loading: an application to Glacial Isostatic Adjustment in Antarctica and Canada. Geophys. J. Int., 192(2), 557-572, 2013.

Andermann, C., Longuevergne, L., Bonnet, S., Crave, A., Davy, P., and Gloaguen, R. : Impact of transient groundwater storage on the discharge of Himalayan rivers. Nat. Geosci., 5(2), 127, 2012.

Barnett, T. P., Adam, J. C., and Lettenmaier, D. P.: Potential impacts of a warming climate on water availability in snow-dominated regions. Nature, 438, 303. doi: 10.1038/nature04141, 2005.

Biemans, H., Siderius, C., Lutz, A., Nepal, S., Ahmad, B., Hassan, T., von Bloh, W., Wijngaard, R., Wester, P., Shrestha, A. and Immerzeel, W.: Importance of snow and glacier meltwater for agriculture on the Indo-Gangetic Plain. Nature Sustainability, 2(7), pp.594-601, 2019.

Björnsson, H., and Venegas, S.: A manual for EOF and SVD analyses of climatic data. CCGCR Report, 97(1), 112-134, 1997.

Bolch, T., Kulkarni, A., Kaab, A., Huggel, C., Paul, F., Cogley, J. G., . . . Stoffel, M.: The State and Fate of Himalayan Glaciers. Science, 336(6079), 310-314. doi: 10.1126/science.1215828, 2012.

Bookhagen, B., and Burbank, D. W.: Toward a complete Himalayan hydrological budget: Spatiotemporal distribution of snowmelt and rainfall and their impact on river discharge. J. Geophys. Res., 115(F3). doi: 10.1029/2009jf001426, 2010.

Brun, F., Berthier, E., Wagnon, P., Kääb, A., and Treichler, D.: A spatially resolved estimate of High Mountain Asia glacier mass balances from 2000 to 2016. Nat. Geos. doi: 10.1038/ngeo2999, 2017.

Chen, J. L., Wilson, C. R., Li, J., and Zhang, Z.: Reducing leakage error in GRACE-observed long-term ice mass change: a case study in West Antarctica. J. Geodesy, 89(9), 925-940. doi: 10.1007/s00190-015-0824-2, 2015.

Chen, X., Long, D., Hong, Y., Zeng, C., and Yan, D.: Improved modeling of snow and glacier melting by a progressive two-stage calibration strategy with GRACE and multisource data: How snow and glacier meltwater contributes to the runoff of the Upper Brahmaputra River basin? Water Resour. Res., 53(3), 2431-2466, 2017.

Cheng, M., Ries, J. C., and Tapley, B. D.: Variations of the Earth's figure axis from satellite laser ranging and GRACE. J. Geophys. Res., 116(B1). doi: 10.1029/2010jb000850, 2011.

Cogley, J., Hock, R., Rasmussen, L., Arendt, A., Bauder, A., Braithwaite, R., and Nicholson, L.: Glossary of glacier mass balance and related terms. IHP-VII technical documents in hydrology, 86, 965, 2011.

Das, I., and Sarwade, R.: Snow depth estimation over north-western Indian Himalaya using AMSR-E. Int. J. Remote Sens., 29(14), 4237-4248, 2008.

Dehecq, A., Gourmelen, N., Gardner, A. S., Brun, F., Goldberg, D., Nienow, P. W., and Trouvé, E.: Twenty-first century glacier slowdown driven by mass loss in High Mountain Asia. Nat. Geos., 12(1), 22-27. doi: 10.1038/s41561-018-0271-9, 2018.

Dobslaw, H., Bergmann-Wolf, I., Dill, R., Poropat, L., and Flechtner, F.: AOD1B Product Description Document for Product Release 06 (Rev. 6.1, October 19, 2017), 2017.

Farr, T. G., Rosen, P. A., Caro, E., Crippen, R., Duren, R., Hensley, S., and Roth, L.: The shuttle radar topography mission. Rev. Geophys., 45(2), 2007.

Gardelle, J., Berthier, E., Arnaud, Y., and Kääb, A.: Region-wide glacier mass balances over the Pamir-Karakoram-Himalaya during 1999andndash;2011. The Cryosphere, 7(4), 1263-1286. doi: 10.5194/tc-7-1263-2013, 2013.

Gardner, A. S., Moholdt, G., Cogley, J. G., Wouters, B., Arendt, A. A., Wahr, J., and Paul, F.: A Reconciled Estimate of Glacier Contributions to Sea Level Rise: 2003 to 2009. Science, 340(6134), 852-857. doi: 10.1126/science.1234532, 2013.

Hall, D., Salomonson, V., and Riggs, G.: MODIS/Terra snow cover daily L3 global 500m grid. Version 5. Boulder, Colorado USA: National Snow and Ice Data Center, 2006.

Huffman, G., Bolvin, D., Braithwaite, D., Hsu, K., Joyce, R., and Xie, P.: Tropical Rainfall Measuring Mission (TRMM) (2011), TRMM (TMPA/3B43) Rainfall Estimate L3 1 month 0.25 degree x 0.25 degree V7, Greenbelt, MD, Goddard Earth Sciences Data and Information Services Center (GES DISC). Retrieved from: http://dx.doi.org/10.5067/TRMM/TMPA/MONTH/7, 2014.

Humphrey, V., Gudmundsson, L., and Seneviratne, S. I.: Assessing Global Water Storage Variability from GRACE: Trends, Seasonal Cycle, Subseasonal Anomalies and Extremes. Surv. Geophys., 37(2), 357-395. doi: 10.1007/s10712-016-9367-1, 2016.

Huss, M.: Density assumptions for converting geodetic glacier volume change to mass change. The Cryosphere, 7(3), 877-887, 2013.

Huss, M., Bookhagen, B., Huggel, C., Jacobsen, D., Bradley, R. S., Clague, J. J., . . . Winder, M.: Toward mountains without permanent snow and ice. Earth's Future, 5(5), 418-435. doi: doi:10.1002/2016EF000514, 2017.

Immerzeel, W. W., Van Beek, L. P., and Bierkens, M. F.: Climate change will affect the Asian water towers. Science, 328(5984), 1382-1385, 2010.

Jacob, T., Wahr, J., Pfeffer, W., and Swenson, S.: Recent contributions of glaciers and ice caps to sea level rise. Nature, 482(7386): 514-518. DOI:10.1038/nature10847, 2012

Jansson, P., Hock, R., and Schneider, T.: The concept of glacier storage: a review. J. Hydrol., 282(1), 116-129. doi: https://doi.org/10.1016/S0022-1694(03)00258-0, 2003.

Kääb, A., Berthier, E., Nuth, C., Gardelle, J., and Arnaud, Y.: Contrasting patterns of early twenty-first-century glacier mass change in the Himalayas. Nature, 488(7412), 495-498. doi: 10.1038/nature11324, 2012.

Kääb, A., Treichler, D., Nuth, C., and Berthier, E.: Brief Communication: Contending estimates of 2003–2008 glacier mass balance over the Pamir–Karakoram–Himalaya. The Cryosphere, 9(2), 557-564. doi: 10.5194/tc-9-557-2015, 2015.

Kaser, G., Großhauser, M., and Marzeion, B.: Contribution potential of glaciers to water availability in different climate regimes. P. Natl. Acad. Sci. USA, 2010.

Kusche, J., Schmidt, R., Petrovic, S., and Rietbroek, R.: Decorrelated GRACE time-variable gravity solutions by GFZ, and their validation using a hydrological model. J. Geodesy, 83(10), 903-913. doi: 10.1007/s00190-009-0308-3, 2009.

Lutz, A. F., Immerzeel, W. W., Shrestha, A. B., and Bierkens, M. F. P.: Consistent increase in High Asia's runoff due to increasing glacier melt and precipitation. Nat. Clim. Change, 4(7), 587-592. doi: 10.1038/Nclimate2237, 2014.

Matsuo, K., and Heki, K.: Time-variable ice loss in Asian high mountains from satellite gravimetry. Earth Planet. Sc. Lett., 290(1-2), 30-36. doi: 10.1016/j.epsl.2009.11.053, 2010.

~~Maussion, F., Scherer, D., Mölg, T., Collier, E., Curio, J., and Finkelnburg, R.: Precipitation seasonality and variability over the Tibetan Plateau as resolved by the High Asia Reanalysis. J. Climate, 27(5), 1910-1927, 2014.~~

Ohmura, A.: Observed Mass Balance of Mountain Glaciers and Greenland Ice Sheet in the 20th Century and the Present Trends. Surv. Geophys., 32(4), 537-554. doi: 10.1007/s10712-011-9124-4, 2011.

Ohno, H., Ohata, T. and Higuchi, K.: The influence of humidity on the ablation of continental-type glaciers. Annals of Glaciology, 16, pp.107-114, 1992.

RGI Consortium.: Randolph Glacier Inventory – A Dataset of Global Glacier Outlines: Version 6.0: Technical Report, Global Land Ice Measurements from Space, Colorado, USA. Digital Media, 2017.

Rodell, M., Houser, P. R., Jambor, U., Gottschalck, J., Mitchell, K., Meng, C. J., . . . Toll, D.: The Global Land Data Assimilation System. B. Am. Meteorol. Soc., 85(3), 381-394. doi: 10.1175/bams-85-3-381, 2004.

Sakai, A., and Fujita, K.: Contrasting glacier responses to recent climate change in high-mountain Asia. Sci. Rep., 7(1), 13717. doi: 10.1038/s41598-017-14256-5, 2017.

Shamsudduha, M., Taylor, R., and Longuevergne, L.: Monitoring groundwater storage changes in the highly seasonal humid tropics: Validation of GRACE measurements in the Bengal Basin. Water Resour. Res., 48(2), 2012.

Sun, W., Wang, Q., Li, H., Wang, Y., Okubo, S., Shao, D., Liu, D., and Fu, G.: Gravity and GPS measurements reveal mass loss beneath the Tibetan Plateau: Geodetic evidence of increasing crustal thickness. Geophys. Res. Lett., 36. DOI:10.1029/2008gl036512, 2009.

Swenson, S., Chambers, D., and Wahr, J.: Estimating geocenter variations from a combination of GRACE and ocean model output. J. Geophys. Res.: Solid Earth (1978–2012), 113(B8), 2008.

Swenson, S., and Wahr, J.: Post-processing removal of correlated errors in GRACE data. Geophys. Res. Lett., 33(8). doi: 10.1029/2005gl025285, 2006.

Tanck, R., and Fazani, A.: Damming Tibet's Yarlung Tsangpo-Brahmaputra and other South Asian rivers. Retrieved May 5, 2019, from http://tibetanplateau.blogspot.com/2010/05/damming-tibets-yarlung-tsangpo.html, 2010.

Tapley, B. D., Bettadpur, S., Ries, J. C., Thompson, P. F., and Watkins, M. M.: GRACE measurements of mass variability in the Earth system. Science, 305(5683), 503-505, 2004.

Treichler, D., and Kääb, A.: Snow depth from ICESat laser altimetry—A test study in southern Norway. Remote Sens. Environ., 191, 389-401, 2017.

Wang, Q., Yi, S., Chang, L., and Sun, W.: Large-Scale Seasonal Changes in Glacier Thickness Across High Mountain Asia. Geophys. Res. Lett., 44, 10427-10435, 2017.

Wijngaard, R., Lutz, A., Nepal, S., Khanal, S., Pradhananga, S., Shrestha, A. and Immerzeel, W.: Future changes in hydro-climatic extremes in the Upper Indus, Ganges, and Brahmaputra River basins. PloS one, 12(12), 2017.

Wouters, B., Chambers, D., and Schrama, E. J. O.: GRACE observes small-scale mass loss in Greenland. Geophys. Res. Lett., 35(20). doi: 10.1029/2008gl034816, 2008.

Wu, G., Guan, Y., Liu, Y., Yan, J., and Mao, J.: Air–sea interaction and formation of the Asian summer monsoon onset vortex over the Bay of Bengal. Clim. Dynam., 38(1-2), 261-279. doi: 10.1007/s00382-010-0978-9, 2011.

Yang, W., Yao, T., Guo, X., Zhu, M., Li, S., and Kattel, D. B.: Mass balance of a maritime glacier on the southeast Tibetan Plateau and its climatic sensitivity. J. Geophys. Res.: Atmospheres, 118(17), 9579-9594. doi: 10.1002/jgrd.50760, 2013.

Yao, T., Thompson, L., Yang, W., Yu, W., Gao, Y., Guo, X., and Joswiak, D.: Different glacier status with atmospheric circulations in Tibetan Plateau and surroundings. Nat. Clim. Change, 2(9), 663-667. doi: 10.1038/nclimate1580, 2012.

Yi, S., and Sun, W.: Evaluation of glacier changes in high-mountain Asia based on 10 year GRACE RL05 models. J. Geophys. Res.: Solid Earth, 119(3), 2504-2517. doi: 10.1002/2013jb010860, 2014.

Yi, S., Sun, W., Feng, W., and Chen, J.: Anthropogenic and climate-driven water depletion in Asia. Geophys. Res. Lett., 43(17), 9061-9069, 2016.

Zhang, L. L., Su, F. G., Yang, D. Q., Hao, Z. C., and Tong, K.: Discharge regime and simulation for the upstream of major rivers over Tibetan Plateau. J. Geophys. Res.-Atmospheres, 118(15), 8500-8518. doi: 10.1002/jgrd.50665, 2013.

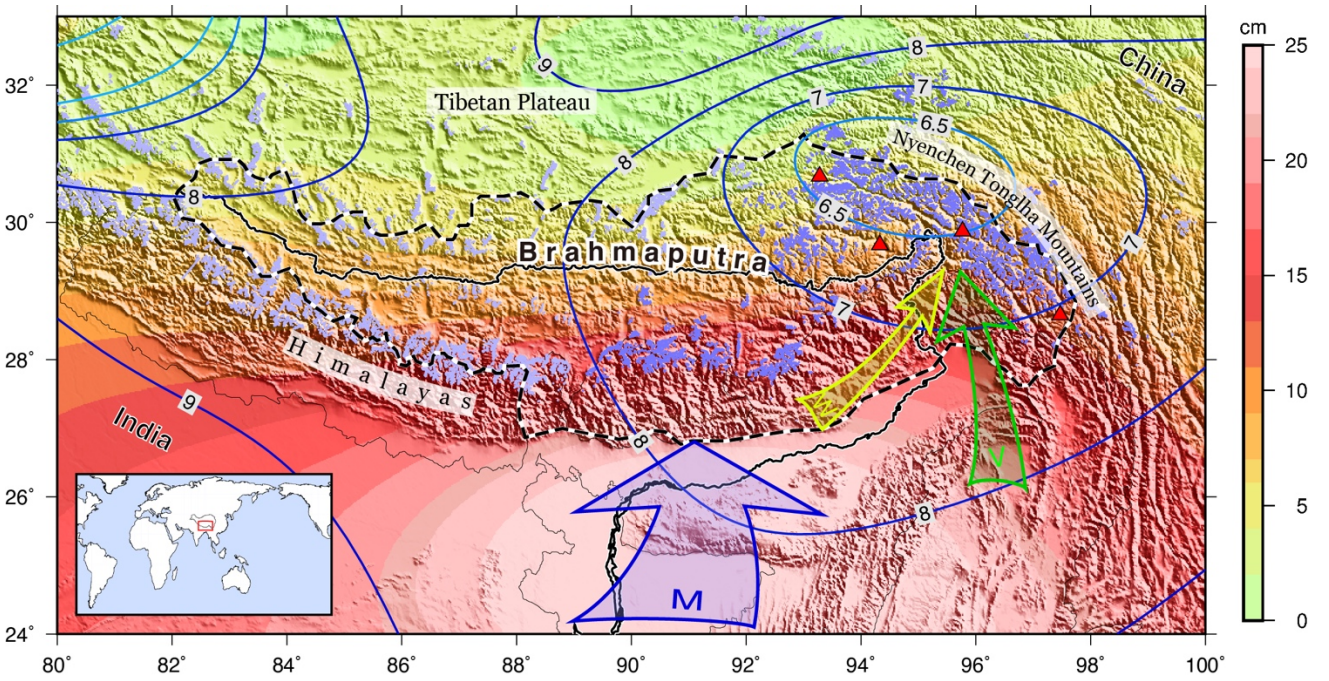

Figure 1. Geographic environment of the upper Brahmaputra Basin. The boundary of the basin is outlined by the black dashed line. The violet areas in the plateau represent mountain glaciers, but only the darker ones (9,679 km^2 in total) are studied here. The background color shows the amplitudes of annual variation in terms of equivalent water height from GRACE, and their peak months (the month with the peak value in a year) are indicated using contours (e.g. 9 means September). The red triangles mark the location of four meteorological stations. The colored arrows illustrate major climatic factors influencing this region (M: Indian Monsoon; W: Westerly winds; V: Bay of Bengal Vortex). The red box in the inset map marks the location of the study area.

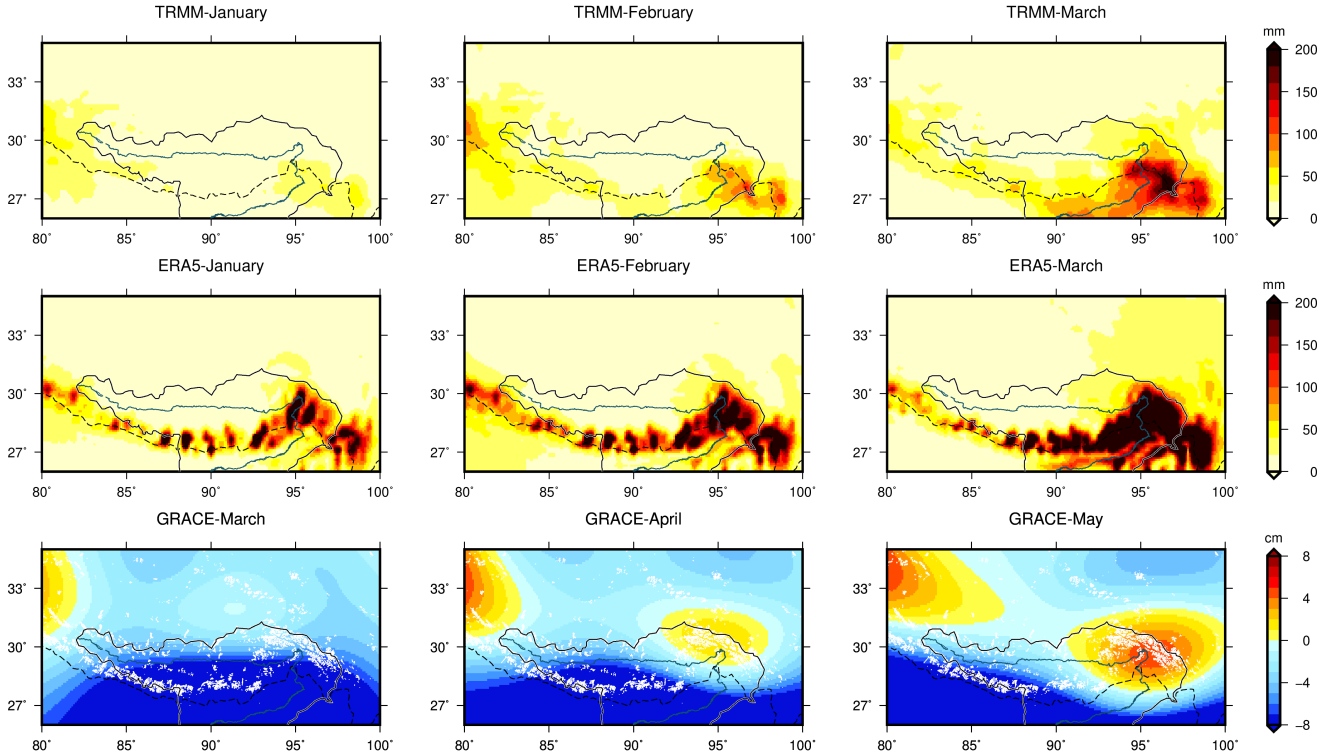

Figure 2. Monthly precipitation from January to March by TRMM and ~~HAR~~ ERA5 and mass anomalies from March to May by GRACE. The Brahmaputra and its basin boundary are marked. The white shaded areas in the bottom plots represent glacier distribution.

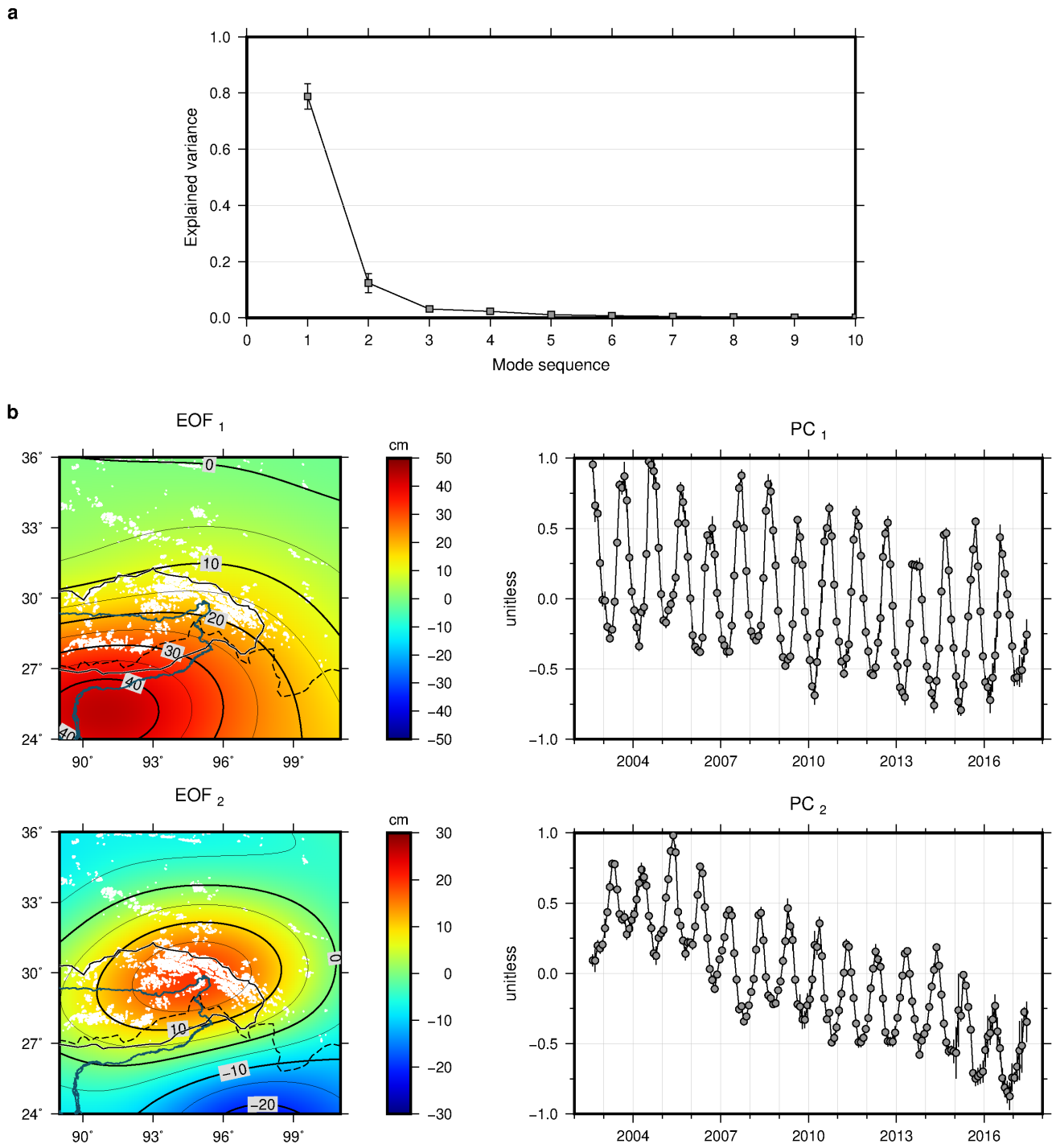

Figure 3. EOF decomposition of GRACE observations in the form of EWH in the study region. Six combinations are averaged to generate these plots and uncertainties are estimated based on the dispersions. (a) Weight of the first 10 components. (b) Spatial distribution (EOF) and temporal variation (PC) of the first two components. The white shaded areas represent glacier distribution.

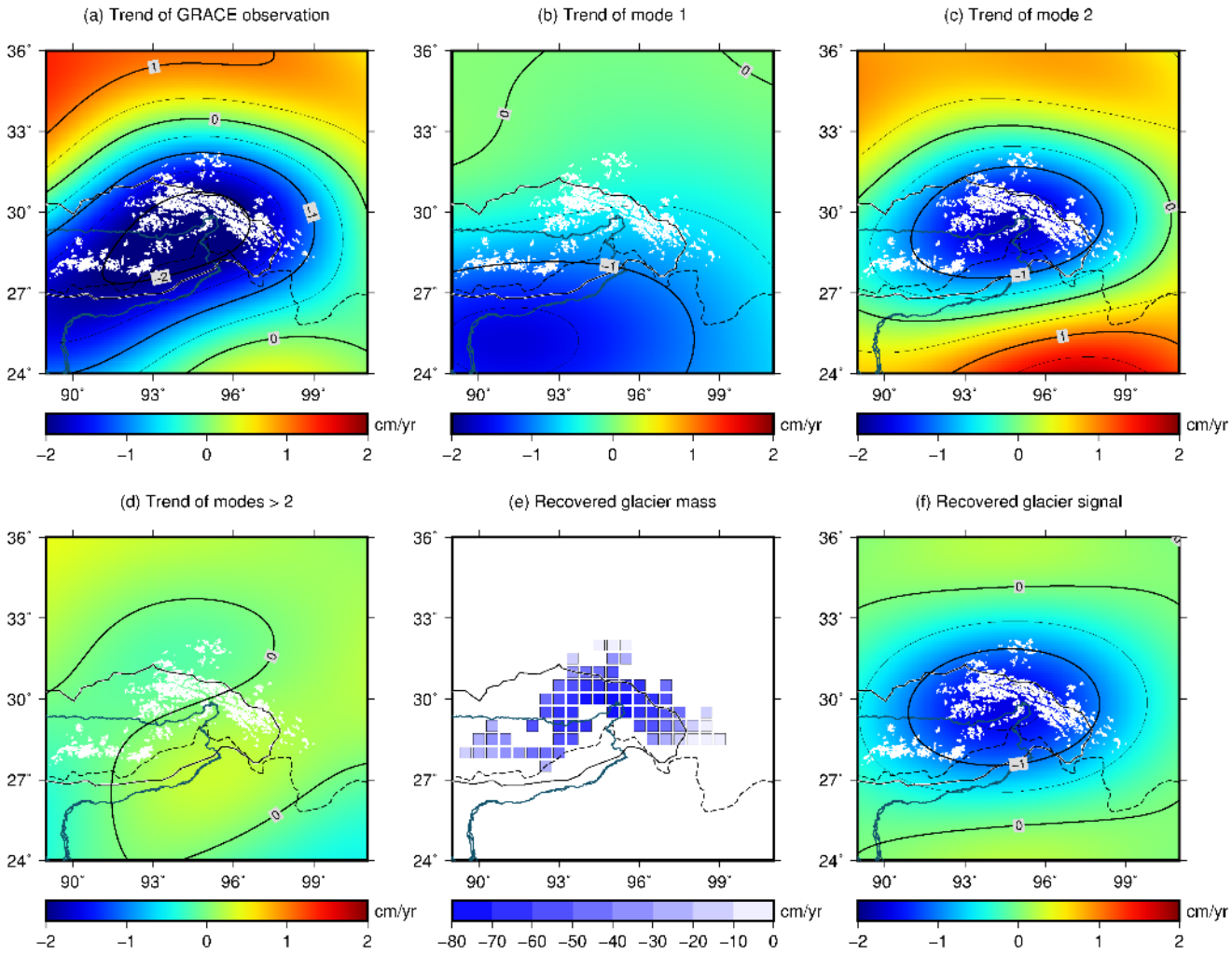

Figure 4. Trend of GRACE signals and the GS mass estimation. The CSR product with DDK4 filter is used here. (a) the trend of GRACE EWH observations between Aug 2002 and June 2017, is decomposed into (b), (c) and (d). Using the mass changes shown in (e), we obtained (f) by the forward modelling method to reproduce (c). The white shaded areas represent glacier distribution. The black solid curve marks the basin boundary and the dashed curve marks the plateau boundary.

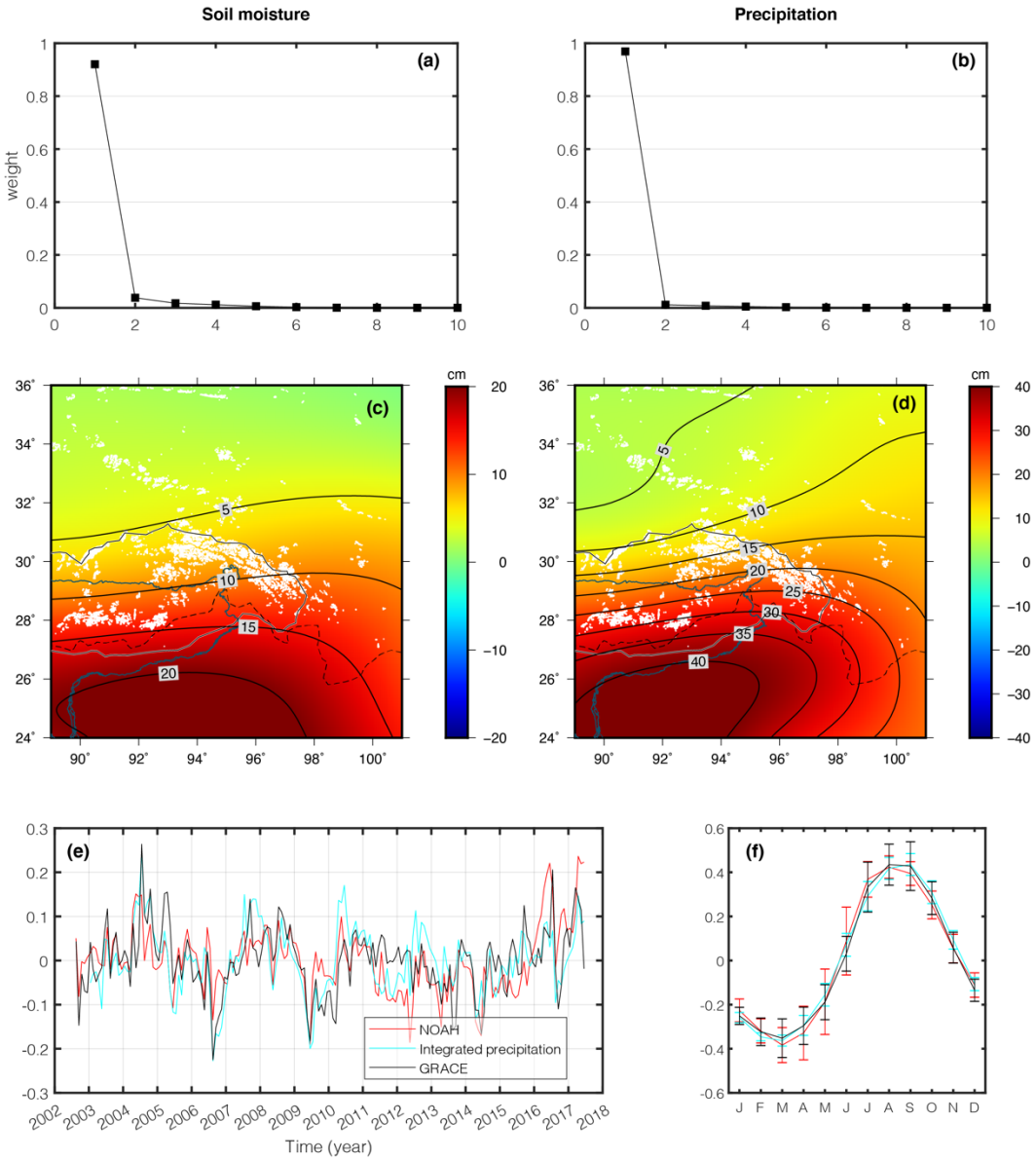

Figure 5. EOF analysis of soil moisture using GLDAS/NOAH (a, c) and of precipitation using TRMM (b, d). The weights of the first 10 modes are shown in the upper panels. The first EOFs and PCs are shown in the middle and bottom panels. The PCs are separated into detrended interannual (e) and annual (f) for better comparison.

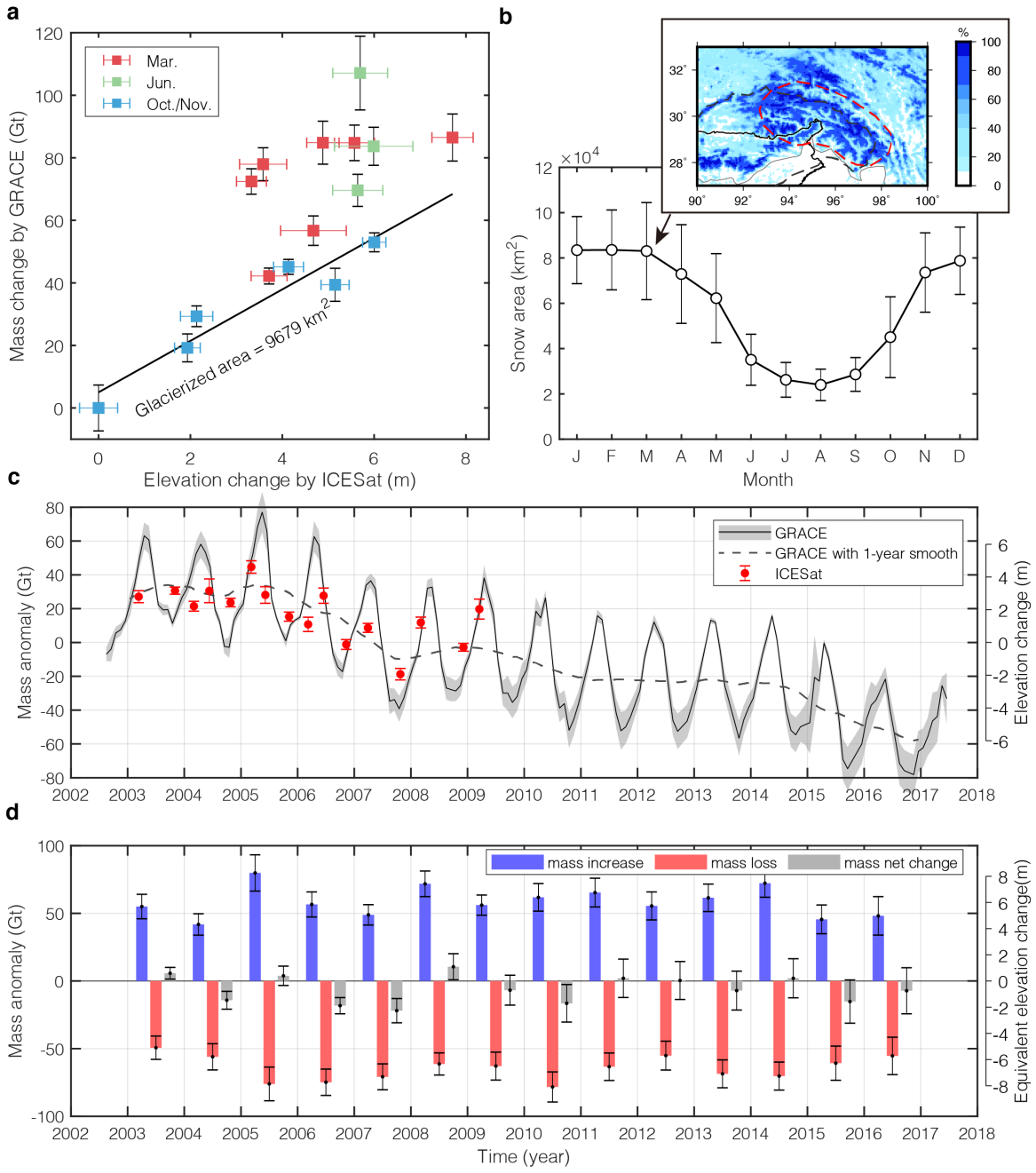

Figure 6. GS mass balance in the SETP. (a) GS mass change by GRACE as a function of elevation change from ICESat. The values are anomalies relative to the minimum in October 2007. (b) Seasonal snow coverage changes. The error bars are calculated by the dispersions in the same month among years from 2003 to 2016. The coverage in March is given in the inset. The red dashed circle marks the region used for the calculation of snow area. (c) Time series of GS mass change estimated by GRACE and glacier mas change by ICESat. The glacierized area of 9,679 km^2 is used to convert thickness change into mass change. (d) Annual mass increase/decrease from 2003 to 2016 by GRACE.

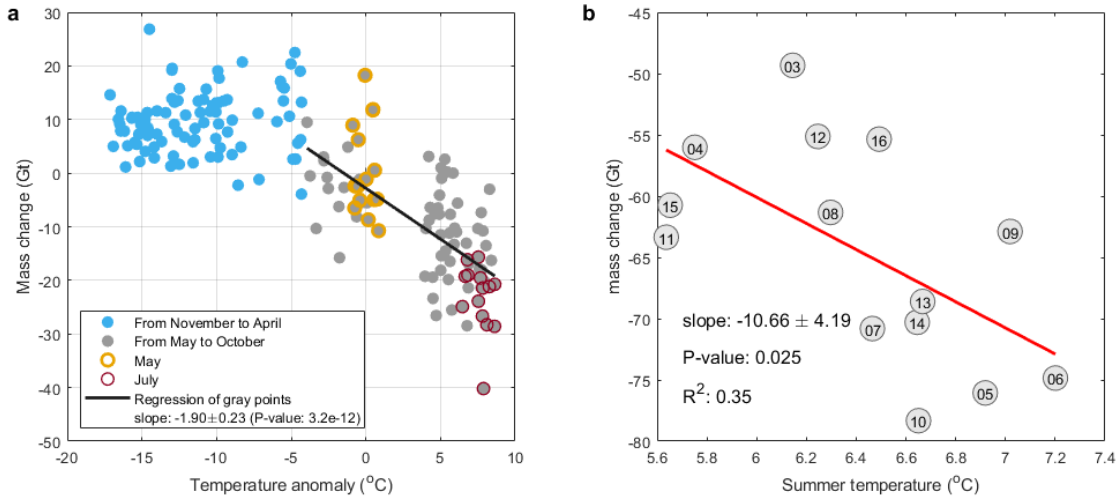

Figure 7. Regression between mass change and temperature. (a) Monthly mass changes as a function of monthly temperature anomalies. (b) Linear regression between annual mass decreases and summer temperatures. The number in the circle represents the year of the data (e.g. "15" shows 2015).

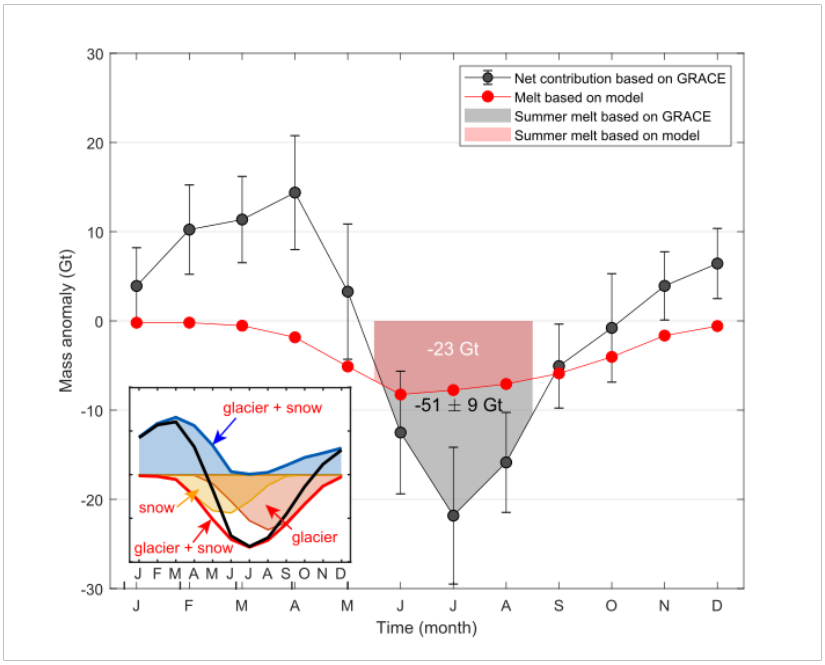

Figure 8. Monthly mass change from GS in the upper Brahmaputra Basin estimated by GRACE and by the model of Lutz et al. (2014). Negative values mean a net increase of meltwater (i.e., more glacier and snow melt than accumulation). Note that Lutz's model only estimated the melt component, while GRACE detects the net change including both melt and accumulation. The estimates of summer melt are annotated. A schematic diagram of seasonal mass balance is shown in the inset (Blue text represents mass accumulation, red represents ablation, and the black curve represents the net change). Note 85% of the meltwater in our study region runs into the Brahmaputra and this amount comes from 83% of glacierized area in this basin, we scale our result by 1×0.85/0.83 to be comparable with the model estimate.

Table 1. Previous model-based estimates of meltwater contribution to the Brahmaputra discharge.

Study literature	Time span	Drainage area (km^2)	Amount of meltwater (w.e. km^3 yr^{-1})	Total discharge (km^3 yr^{-1})	Meltwater/total discharge (%)
Immerzeel et al. 2010	2000–2007	525,797	62	230	27
Bookhagen and Burbank, 2010	1998–2007	255,929	55	161	34
Zhang et al., 2013	1961–1999	201,200*	20	58	35
Lutz et al., 2014	1998–2007	360,000	43	131	33
Huss et al., 2017	2002–2011**	533,000	138	732	19
Chen et al., 2017~~b~~	2003–2014	240,000*	12	60	21

*: Exclude large parts of the NTM region.~~The NTM is almost not included.~~

**: The time spans vary a bit in different datasets.

Table 2. GRACE error sources for the long-term trend. (Unit: Gt/yr)

Source	Error	Remark
Linear Fit	0.14	Calculated from fitting residuals of a linear and trigonometric model
Data solution and smoothing errors	0.44	Estimated from the dispersion among CSR, GFZ and JPL with DDK4/G300+P4M6
Leakage error	0.51	The average peak date may vary from May 6th to May 16th
GIA	0.02	Difference between results with and without A's GIA model (A et al., 2013)
LIA	0.20	The total LIA effect in the whole Himalaya range and southeastern Tibet is -1±1 Gt/yr
Denudation	0.32	The total denudation effect in the eastern and southeastern Tibetan Plateau is 0.8 km^3/yr
Total	0.78	